Summer 2017

Urban Detention Basin Contamination with Polycyclic Aromatic Hydrocarbons (PAHs) and Metals

Holly Marie Duff
Missouri State University, Duff013@live.missouristate.edu

URBAN DETENTION BASIN CONTAMINATION WITH POLYCYCLIC AROMATIC HYDROCARBONS (PAHS) AND METALS

A Masters Thesis

Presented to

The Graduate College of

Missouri State University

In Partial Fulfillment

Of the Requirements for the Degree

Master of Science, Geospatial Sciences in Geography, Geology, and Planning

By

Holly Marie Duff

August 2017

URBAN DETENTION BASIN CONTAMINATION WITH POLYCYCLIC AROMATIC HYDROCARBONS (PAHS) AND METALS

Geography, Geology, and Planning

Missouri State University, August 2017

Master of Science

Holly Marie Duff

ABSTRACT

Polycyclic aromatic hydrocarbons (PAHs) are organic compounds that can be toxic to wildlife and humans when released to the environment. Coal-tar sealants, which are applied to parking lots or driveways, contribute up to 1,000 times more PAHs than alternative sealants. Over time, these sealants abrade and are transported into drainage networks. Coal-tar sealants are currently used in Springfield, Missouri, however the extent of PAH contamination throughout urban drainage systems is unclear. This study focused on PAH contamination within an urban detention basin on the Missouri State University campus which receives runoff from several coal-tar sealed parking lots. Sediment samples collected within the basin and catchment were analyzed for PAHs, metals, grain size, and organic matter. Findings show that 65% of the samples exceed the defined toxicity limit of 22,800 μg/kg PAHs. Channel sediment collected within close proximity to inlets or outlets contained significantly higher concentrations compared to basin soil areas adjacent to concrete trickle channels. While contaminated depths were typically < 5 cm, high sedimentation areas showed a decreasing trend in PAH concentrations to depths of 25-35 cm. Although toxic levels of PAHs were found in the detention basin, < 1% of PAHs entering the catchment are being stored within the basin.

KEYWORDS: polycyclic aromatic hydrocarbons, coal-tar sealant, detention basin, geochemistry, Missouri

This abstract is approved as to form and content

_____

Dr. Robert Pavlowsky
Chairperson, Advisory Committee
Missouri State University

URBAN DETENTION BASIN CONTAMINATION WITH POLYCYCLIC AROMATIC HYDROCARBONS (PAHS) AND METALS

By

Holly Marie Duff

A Masters Thesis
Submitted to the Graduate College
Of Missouri State University
In Partial Fulfillment of the Requirements
For the Degree of Master of Science, Geospatial Sciences in Geography, Geology, and Planning

August 2017

Approved:

_____
Robert Pavlowsky, PhD

_____
Melida Gutierrez, PhD

_____
Jun Luo, PhD

_____
Julie Masterson, PhD: Dean, Graduate College

ACKNOWLEDGEMENTS

I would like to thank Dr. Robert Pavlowsky, Dr. Melida Gutierrez, and Dr. Jun Luo for their assistance in the completion of my thesis. I would also like to thank Marc Owen, Chad Cooper, Rachael Bradley, Kayla Geier, Matthew Thies, Megan Hente, Thomas Duff, Dr. Gary Michelfelder, and Dr. Matthew Siebert for additional assistance. Additionally, financial assistance for my graduate studies and thesis research was acquired from: The College of Natural and Applied Sciences, Graduate College, Department of Geography, Geology, and Planning, and Ozarks Environmental and Water Resources Institute.

I dedicate this thesis to Tom and Susan Duff and loved ones, for their continuous encouragement and support.

TABLE OF CONTENTS

LIST OF TABLES

LIST OF FIGURES

INTRODUCTION

Polycyclic aromatic hydrocarbons (PAHs) are organic, benzene ring structures that contain double bonds linking hydrogen and carbon molecules (National Research Council (US) Committee on Pyrene and Selected Analogues, 1983; Abdel-Shafy and Mansour, 2016). PAHs are known carcinogens that are toxic to terrestrial and aquatic species and do not easily degrade under natural conditions (Boffetta et al., 1997; Eisler, 1987; Quantin et al., 2004). While these contaminants are known to be harmful, they are still commonly introduced into the environment from both natural and anthropogenic sources, such as incomplete combustion of fossil fuels and the burning of materials, such as wood or metals (Eisler, 1987; Bixian et al., 2001; Pies et al., 2007; Feng et al., 2007; Abdel-Shafy and Mansour, 2016). A significant contributor of PAHs to urban watersheds since the 1960's in the central and eastern USA are coal-tar sealants (USGS, 2011; Crane, 2013; USGS, 2015). Coal-tar sealants are placed on roads, parking lots, and driveways as a protective coating and to provide an aesthetically appealing appearance (Eisler, 1987; Crane, 2013). These sealants, however, are not permanent and are often eroded and carried away by storm runoff water, needing to be reapplied every three to five years (Guar et al., 2005; Crane, 2013). Sealant particles may also be swept away by wind, carried car or bike tires, or evaporated into the air (Crane, 2013; Eisler, 1987).

Detention basins are prone to receiving and retaining PAH contaminated sediment (Eisler, 1987; Guo, 1997; Motelay-Massei, 2004; Maxted and Shaver, 1998; Birch et al., 2006). Detention basins, dry or wet, are designed to store run off water to limit the amount of water transferred to the local water systems. Dry detention basins, the focus of

this project, are designed to temporarily retain the excess runoff water (Guo, 1997). During this retention period, the water is slowly released into the local drainage system and the sediment transported by the runoff can settle within the detention basin. The settling velocities of sediment particles increase the deposition rates of PAHs in the basin, which decreases the contamination risk to downstream water sources (Birch et al., 2006). However, the end result is that detention basins become a potential hotspot for long-term PAH contamination (Crane, 2013).

PAH Sources and Concerns

Polycyclic aromatic hydrocarbons became a concern due to their pollution of urban stream sediments (Luo et al., 2004). Because they do not easily degrade in the natural environment resulting in the deposition and accumulation within sediment deposits (Quantin et al., 2004; Gan et al., 2009). PAHs are transported throughout the environment by several different methods such as air, water, or automobiles (Crane, 2013; Witt et al., 2014). Their transportation is also dictated by their molecular structure and their remobilization potential (Wolska et al., 2002; Feng et al., 2007). PAH structures vary from two or more fused benzene rings (Haritash and Kaushik, 2009; Choi et al., 2010). As the number of rings increase, the molecular weight rises. The heavier molecules tend to be more resistant to degradation, while molecules with fewer rings are more prone to natural break down, becoming water soluble and being transported throughout the environment (Crane, 2013; Mahler et al.,2014).

PAH Sources. Anthropogenic events are the largest contributor of PAHs to the environment (Pies et al., 2007). Anthropogenic sources may be petrogenic or pyrogenic

(Ahrens and Depree, 2010; Irwin et al., 1997). The pyrogenic PAHs are generated by combustion of materials such as industrial and atmospheric emissions as well as vehicular contamination. Petrogenic PAHs are generated through petroleum contamination (Ahrens and Depree, 2010). Naturally occurring events may introduce PAHs into the environment. These events may be instances such as volcanic eruptions or forest fires (Eisler, 1987; Howsam and Jones, 1988). These sources naturally release PAHs into the atmosphere and surrounding environment, but account for only a small amount of the total PAH accumulation within the ecosystem (Pies et al., 2007; Gu et al., 2003).

Anthropogenic sources may also include pollution from industrial equipment (Bixian et al., 2001; Gu et al., 2003). Industrial equipment may undergo weathering or natural processes which results in the sloughing off of PAHs and other contaminants such as heavy metals (Bixian et al., 2001; Eisler, 1987). Other sources that may introduce PAHs into the environment may be the incomplete combustion of fossil fuel burning, oil contamination, tar, sealant abrasion, and gas production (Bixian et al., 2001; Gu et al., 2003; Feng et al., 2007; Srogi, 2007; Crane, 2013,). PAHs can also be released from residential developments. Sources such as roofing, road paving, and pavement sealing are common sources that introduce PAHs into the ecosystem (Crane, 2013).

PAH Toxicity Concerns. PAHs are considered toxic in the environment. PAH water contamination has been shown to be dangerous to several aquatic species such as wild-brown bullhead catfish and rainbow trout (Baumann and Harshbarger, 1995; Yang et al., 2010). PAHs that are suspended or dissolved in the water column can accumulate in the tissues of aquatic life (Mahler et al., 2015). Aquatic life typically does not have the capability to naturally metabolize these toxins, which results in the storage of the PAHs

within the organism's tissues. This may lead to cancer, tumors, or severe illness of aquatic life, which has been affected (Eisler, 1987; Baumann and Harshbarger, 1995; Crane, 2013). Polycyclic aromatic hydrocarbons are also toxic to humans, namely to those who are exposed to industrial working areas or careers with road paving or sealing (Boffetta et al., 1997; Srogi, 2007). People who are exposed to significant amounts of PAHs may develop lung, skin, or bladder cancer (Boffetta et al., 1997; Choi et al., 2010; Srogi, 2007). Industrial jobs pose a higher risk because toxins are commonly emitted into the air (Eisler, 1987). Inhalation is one of the primary ways that PAH particles enter the body; this often leads to an increase in lung or throat cancer (Boffetta et al., 1997; Irwin et al., 1997).

Controlling Factors of PAH Mobility

PAH mobility potential in urban streams is controlled by molecular weight, duration of suspension within the water, and potential for storage in floodplain and basin deposits (Wolska et al., 2002; Feng et al., 2007).

Molecular Structure. PAHs vary in molecular structure, ranging from 2 or more benzene rings (Haritash and Kaushik, 2009). The toxicity levels and molecular weight of PAHs are structurally dependent (Choi et al., 2010; Srogi, 2007; Irwin et al., 1997). The EPA_{16} PAHs found to be carcinogenic were those with ring counts of 4-6, whereas PAHs considered to be non-carcinogenic were those with 2-3 benzene rings (Srogi, 2007; Agency for Toxic Substances and Disease Registry, 2013). As the molecular weight rises with the increased number of rings, the individual structures become more resilient to natural degradation, dissolution in water, and volatility (Khadhar, et al., 2010; Ahrens

and Depree, 2010; Mahler, et al., 2014). The decrease in degradation results in the storage of these organic particles within the environment, whereas if the ring number is much lower it has an increased chance of degradation and becoming water-soluble and transported throughout the environment (Crane, 2013; Mahler, et al., 2014). By becoming part of an aqueous solution, the contaminant may be more easily transported by water flow or evaporation.

Suspension in Water. PAHs mainly enter the water system through atmospheric fallout or urban runoff and are transported in associations with suspended sediments (Wolska et al., 2002; Srogi, 2007). PAHs have a greater remobilization capability if they are suspended in the water column (Wolska et al., 2002; Feng et al., 2007; Santschi et al., 2001). However, in ponds or slow moving water, PAHs commonly settle to the underlying sediment (Feng et al., 2007). Once the suspended particles settle to the bottom, PAH-containing particles begin to mix with and accumulate within local sediment deposits (Feng et al., 2007). To remobilize the PAH molecules, significant amounts of energy must enter the water or sediment system (Feng et al., 2007). This energy may be a severe storm, increase in waves, anthropogenic activity such as boating or swimming, or dredging the bottom sediment (Feng et al., 2007).

Floodplain Contamination. Floodplains retain and store sediment in watersheds (Owen et al., 2013). Human activities such as agricultural and construction may alter the amount and type of sediment distributed to floodplains by increasing or decreasing the sediment supply and transport rate (Jacobson and Coleman, 1986; Lecce and Pavlowsky, 2001). If the pollutants are deposited on a floodplain, they may be released slowly back into the system by erosion or gradual deposition (Yang et al., 2008).

Urban Detention Basins. Detention basins are designed to store excess storm runoff and reduce flood risk in urban watersheds (Maxted and Shaver, 1998; Guo, 1997; Birch et al., 2006). These basins are constructed as a temporary location for water storage to control the peak rate of runoff to downstream water sources (Guo, 1997). Detention basins may also be used as a way to remove contaminants traveling in runoff water before they reach larger water systems through sediment settling and hydrologic or vegetative absorption (Birch et al., 2006). Detention basins, specifically dry ponds, are designed to temporarily store storm runoff for approximately 24-72 hours. During this duration of time, sediment particles transported in the runoff may settle from the water column and begin to accumulate in the basin sediment (Maxted and Shaver, 1998, Guo, 1997). The water that is taken into the detention basin will escape slowly, resulting in the increased levels of sedimentation in the detention basin (Birch et al., 2006). With continued sediment deposits, contaminants may begin to accumulate within the basin sediment (Guo, 1997; Birch et al., 2006).

Storm water detention basins collect and accumulate sediment-borne pollutants such as PAHs or metals (Pies et al., 2007; Fischer et al., 2003). Therefore, pollutants found in detention basin groundwater typically reflect surrounding anthropogenic activity (Fischer et al., 2003). Pollutants stored in basins can leach or percolate to the water table and contaminate local groundwater supplies (Fischer et al., 2003; Bixian et al., 2001; Paul and Meyer, 2001; Crane, 2013).

Larger quantities of PAHs are generally found in regions of higher industrial activity and roadways compared to locations that are primarily used for agricultural purposes (Hoffman et al., 1984; Motelay-Massei et al., 2004). As the amount of

impermeable surfaces, such as roads and parking lots, increase, the amount of runoff in urban watersheds will continue to rise (Paul and Meyer, 2001). The increase of impermeable surfaces results in more flooding events, large and small, as well as higher flow velocities. This results in greater amounts of water and pollutants transported into local waterways (McCarthy and Zachara, 1989).

PAH Distribution in Sediment

PAHs have a non-polar, cyclical, benzene structure (Abdel-Shafy and Mansour, 2016; Li and Chen, 2007). PAHs are unlikely to bind to loose sediment particulates or become water soluble, but they commonly accumulate throughout the basin and stream sediment (Abdel-Shafy and Mansour, 2016). PAHs may be found within the clay (<3.9 μm), silt (62.5-3.9 μm), or sand (2,000-62.5 μm) fractions of soil or sediment (Pavlowsky, 2013). However, some PAHs can adsorb to organic materials or highly organic soils (Srogi, 2007; Abdel-Shafy and Mansour, 2016). PAHs that are carried into the detention basins or streams will settle to the bottom and begin to accumulate. If there are several detention/retention basins or basins which have multiple catchment regions, they are more likely to disperse the amount of sediment, contaminants, and water accumulated within the basins (Birch et al., 2006). With the dispersal of the water and sediment, the basins are less likely to fail (Guo, 1997; Birch et al., 2006).

Coal-Tar Sealants

A large contributor of PAHs into the ecosystem is coal-tar sealants (Crane, 2013). Coal-tar sealants were first recognized as a significant contributor of PAHs in

urban runoff in 2005 (Van Metre and Mahler, 2013). Coal-tar sealants are a protective coating placed on parking lots, sidewalks, or driveways (Crane, 2013; Mahler, et al., 2014). These sealants are used to protect the recently paved surfaces along with providing an aesthetically appealing appearance (Eisler, 1987; Crane, 2013; Mahler et al., 2014). Coal-tar sealants are regularly placed and reapplied on pavement surfaces every three to five years (Crane, 2013). These sealants are not permanent and are prone to being washed away by storm runoff water, swept away by wind, or carried by the tires of vehicles (Figure 1) (Gaur et al., 2005; Crane, 2013; Pavlowsky, 2013). After they are removed from the primary surface, they are transported to streams or rivers, or local sediment sources (Crane, 2013). Coal-tar sealants have been found to significantly increase the concentration of PAHs entering stormwater compared to regions that were not sealed with coal-tar (EPA, 2016; Mahler et al., 2014). Studies have shown that PAH levels in coal-tar sealants are approximately 50,000,000 µg/kg, compared to asphalt sealants which have an average PAH level of 50,000 µg/kg (USGS, 2011; McKinney, 2012).

PAHs are transported into water systems and surrounding environments through several different methods such as runoff, wind, and anthropogenic activity. Runoff may be from parking lots, roads, or agricultural fields (Hwang and Foster, 2006; Krein and Schorer, 2000; Crane, 2013). The amount and size of the particles transferred depends on the volume and the strength of the water flow (Krein and Schorer, 2000). Another way that PAHs are transported is by wind (Crane, 2013; Witt et al., 2014). Continuous exposure to vehicular friction may result in the abrasion of the coal-tar sealed locations (Figure 1).

A

B

Fig. 1. Parking lot (2011) with coal-tar sealant (A) and (2015) abraded coal-tar sealant (B). Sealant particles formed by weathering and vehicle abrasion are released to local waterways during storm events.

This results in the weakening of the sealant and generation of loose particles (USGS, 2011; Pavlowsky, 2013; Crane, 2013). As the parking lot surface coatings weaken, the particles can be transported by car tires or soles of shoes (Crane, 2013; Ahren and Depree, 2010; Guar et al., 2005). This results in the dispersion of loose PAH-contaminated particles into the watershed including homes and public facilities (USGS, 2011).

Purpose and Objectives

The purpose of this project is to assess the concentrations of sediment PAHs and metals and their spatial distribution in an urban stormwater pond system in Springfield, Missouri, the third largest city in the state. The city government of Springfield has been debating whether or not to ban coal-tar sealants based on the US EPA studies indicating that PAH contamination may be of concern (Pavlowsky, 2013). The project objectives are: (i) quantify the concentrations and patterns of sediment-PAHs in detention basins and evaluate what design, hydrologic, and sediment transport factors influence the spatial variability; (ii) determine the largest contributor of the contaminants; and (iii) evaluate the depth of PAH contamination in sediment/soil cores from the basin.

To understand PAH contamination within the basin, there are different aspects to consider. One being the transport distance from the inlet source point. PAH concentration may undergo dilution of abraded particulates with the introduction of additional water and sediment (Wang et al., 2002; Mahler et al., 2005). PAHs, specifically those with higher molecular weight, have a tendency to be non-volatile and will associate with underlying river or basin sediment and begin to accumulate rather than be transported

(Wang et al., 2002; Ahrens and Depree, 2010; Mahler, et al., 2014). PAHs are not only transported through runoff water but also by car tires and windblown sediment (Crane, 2013; Witt et al., 2014). Therefore, understanding the patterns of PAH deposition may provide insight into their transport or sources. It is also important to consider urban hydrology and catchment source areas. The detention basin is surrounded by two highly traveled roads and a coal-tar sealed parking lot. This parking lot has one outlet into the basin along with the storm runoff, whereas there are two inlets from the roads. Comparing the PAH concentrations throughout these separate locations may distinguish contamination trends from urban runoff in general and coal-tar sealed lots specifically.

Hypotheses

There are six hypotheses guiding this study: (1) It is expected that the highest sedimentation rates and concentrations of PAHs and heavy metals will be located in areas of low flow velocity resulting in areas of high sediment accumulation (McCarthy and Zachara, 1989). These regions would include inlet and outlets of the basin;
(2) The PAH concentration is expected to decrease as the distance increases from the inlet source, due to the settling of the PAH particles into underlying sediment and dilution by cleaner sediment from other sources; (3) The overall PAH concentration is also expected to decrease as elevation above the basin surface increases. PAHs sink and accumulate in the underlying sediment, thus as the elevation increases there is less exposure to water-transported PAHs and flood inundation (Birch et al., 2006). Therefore, PAH concentrations should decrease with distance from the main trickle channel;
(4) PAH concentrations will decrease in locations where there is minimal contribution

from coal-tar parking lots (Van Metre and Mahler, 2013); (5) Individual PAH structures that are expected to be most abundant will be those with higher benzene ring count, compared to those with fewer rings. PAHs with fewer rings are considered to have a lower molecular weight, and are more likely to become water soluble (Crane, 2013; Mahler et al., 2014). In addition, coal-tar sealants and asphalt tend to have high concentrations of higher ring PAHs (Pavlowsky, 2012; Mahler et al., 2014); (6) The downward leaching of PAH contamination into the soil will be low, because the basin is young and sediment-bound PAHs may be relatively stable in the soil or sediment profile.

Benefits

This research will contribute to the general understanding of how PAHs accumulate in sediment from runoff in urban watersheds. Further, this study may also contribute to the understanding of how coal-tar sealants contribute to increased PAH concentration levels. By providing awareness to the public of this increasing problem, remediation of currently existing contaminated areas may be taken more seriously. This may also increase the effort to prevent or limit PAHs from entering the environment.

STUDY AREA

The location at which this project takes place is in Springfield, Missouri on the Missouri State University (MSU) campus (Figure 2). The MSU campus has constructed several storm water detention basins, which receive storm runoff and road inlet drainage (Missouri State University Facilities Management). One basin specifically was chosen for study in the south east corner of the campus (Figure 5). This basin was selected as the primary study area due to its close proximity with a coal-tar sealed parking lot and the significant amount of water transported into and out of the basin.

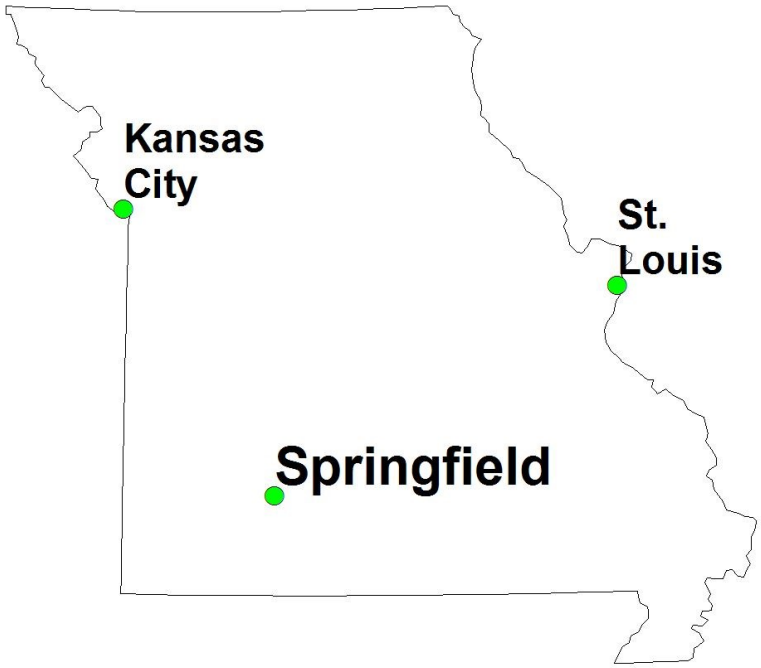

Fig. 2. Location of Springfield, Missouri

Springfield, Missouri is located within the Springfield Plateau of the Ozark Highlands Province (Missouri Department of Natural Resources, 2015). The Ozark Highlands Province is approximately 70,000 square miles, reaching into regions of Kansas, Arkansas, Missouri, and Oklahoma (Westerman, et al., 2016). The stormwater basin drains to Fassnight Creek, to Wilson Creek, and then finally to James River in Greene County, Missouri (Figure 3) (Kiner and Vitello, 2016).

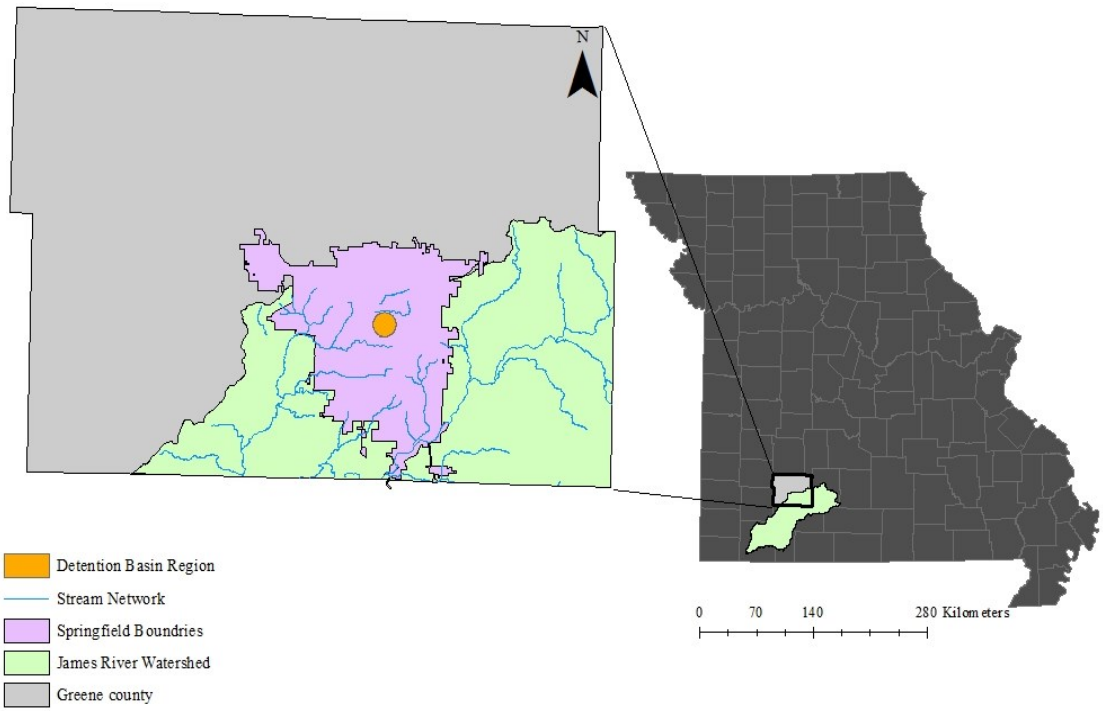

Fig. 3. Greene Country and Springfield portion of James River Watershed

Geology

Located in the Southwestern portion of the Ozark Highlands Province, the Springfield Plateau is the uppermost hydrogeologic layer within this water system. The Springfield Plateau is primarily Mississippian limestone and chert. This specific aquifer

has a median depth of approximately 68 meters below land surface and a maximum thickness of 69 meters (Westerman, et al., 2016). The primary rock types found are the Burlington and Keokuk limestone and chert (Westerman et al., 2016). Also commonly found in the Southern Missouri region of the aquifer are karst features. Due to the abundant amounts of limestone in the region, karst development is a common occurrence (Easterbrook, 1999).

Karst features such as sinkholes and caves, are created by the dissolution of the limestone by rock-water interaction (Cardell, et al., 2008). Limestones are a calcium-carbonate rock, which is easily weathered away primarily by chemical erosion (Easterbrook, 1999; Han and Liu, 2004). This may result in caves, sinkholes, ground subsidence, groundwater contamination, cracks, fissures, and unstable surfaces (Cardell et al., 2008). These features are common within the Springfield, Missouri location. Features such as these may also add to the additional contamination and transportation of contaminants through the excess transportation of runoff groundwater into local aquifer systems (McCarthy and Zachara, 1989; Easterbrook, 1999).

Detention Basin Drainage Area

Detention basin areas and elevations were calculated in ArcGIS using the 10.4 version. The area covered by the central water retention portion of the basin is approximately 4,200 m^2 and the entire detention basin area is approximately 14,000 m^2. The detention basin has a range in elevation of approximately four meters (395.2-399.1 meters). Areas of lowest elevation were found in the central basin as well as the trickle channels (Figure 4).

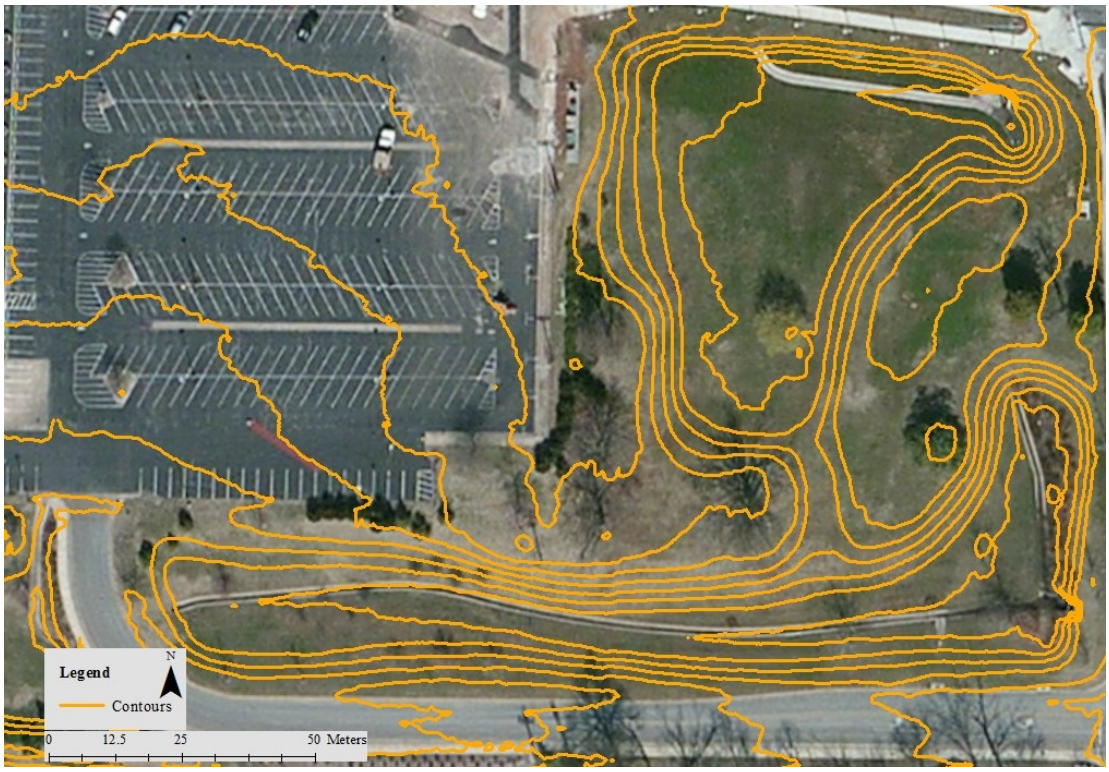

Fig. 4. The elevation changes throughout detention basin (0.4 meter contour interval)

The drainage area flowing into the basin is approximately 0.22 km^2 and incorporates segments of Grand Street, National Avenue, the eastern portion of the MSU campus, and the adjacent coal-tar sealed parking lot (Figure 5; Table 2). The coal-tar sealed parking lot within close proximity is the joined lot 22 and 24 and is approximately 0.03 km^2 in surface area (Table 2).

This basin has three inlet locations and primarily receives runoff from segments of Grand Street, National Avenue, the eastern portion of the MSU campus, and the nearby coal-tar sealed parking lot (Figure 5). Two inlets are from roadway drainage systems and one from the coal-tar sealed lot. The first roadway drainage system is located on Grand Street and the second found on the corner of Grand Street and National Avenue. The third inlet is a trickle channel with direct collection of runoff from the

nearby coal-tar sealed parking lot. The runoff contributed by lot 22 and 24 primarily enters through the trickle channel inlet on the West side of the basin. The single drainage outlet is located in the southeast corner of the study basin. This outlet is the primary exit for any excess runoff water.

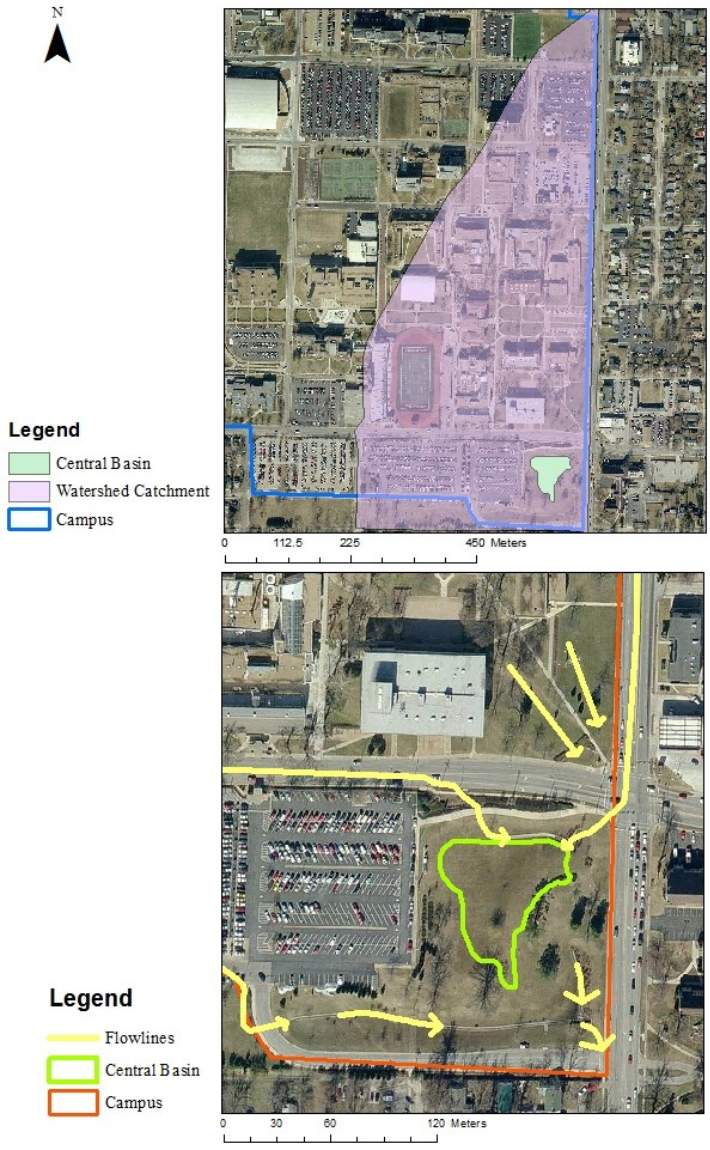

Fig. 5. Basin runoff catchment region and flow patterns of basin

The local soil series contributing to the basin are the Wanda silt-loam and the Creldon silt-loam (Figure 6) (USDA, 2016). The basin watershed catchment borders the

Sacville soil series, which resides to the SE of the basin. The Wanda silt-loam is comprised of fine, silty, active materials as well as cherty-limestone (National Coorperative Soil Survey, 2004). The Creldon is similarly composed of fine and active materials, but has a clayey cherty composition as well (National Cooperative Soil Survey, 2006).

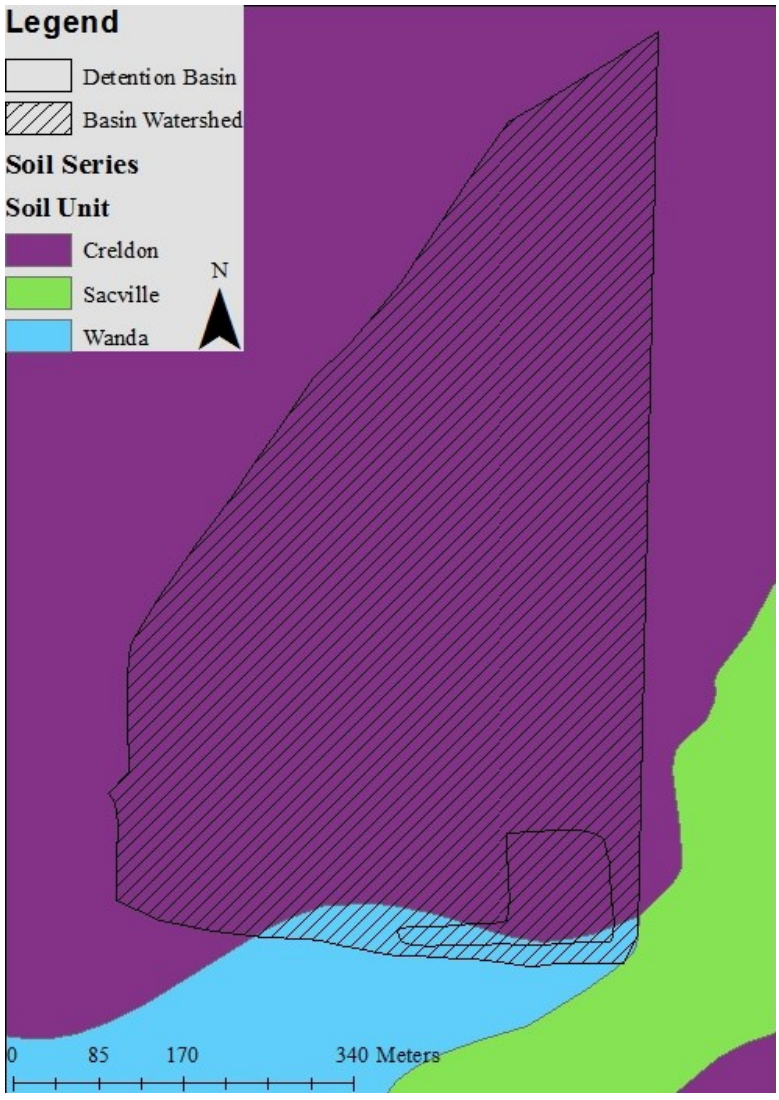

Fig. 6. The soil series of the study basin and surrounding regions

Basin History

Prior to the construction of the detention basin, houses and parking lots occupied the study basin property (Earth Explorer). Aerial photos from February 1990 revealed that the basin was comprised primarily of parking lots and houses (Figure 7). By 1996, there were still parking lots and homes, but there was more groundcover (Earth Explorer). The detention basin was constructed in 1999 (MSU Facilities Management). The adjacent parking lot, Lot 24, was expanded in 1980 with a second expansion occurring in 1982. The corresponding lot 22 was not built until 1985 and was expanded in 1986 (MSU Facilities Management).

No significant changes have been made to the basin since it was constructed (Figure 8), aside from minor disturbances such as dredging (Missouri Grounds Management). Image results are based on the most recent LiDAR image of Springfield (2012). The most recent disturbances to the basin occurred in March, 2016. Inlet and outlet regions that had filled with sediment were dredged in order to allow greater flow out of the basin. Approximately 3.8 m^3 of sediment were removed from the drainage ways within the basin (MSU Grounds Management). This was performed after the initial September 2015 sampling occurred, but prior to the 2016 core sampling.

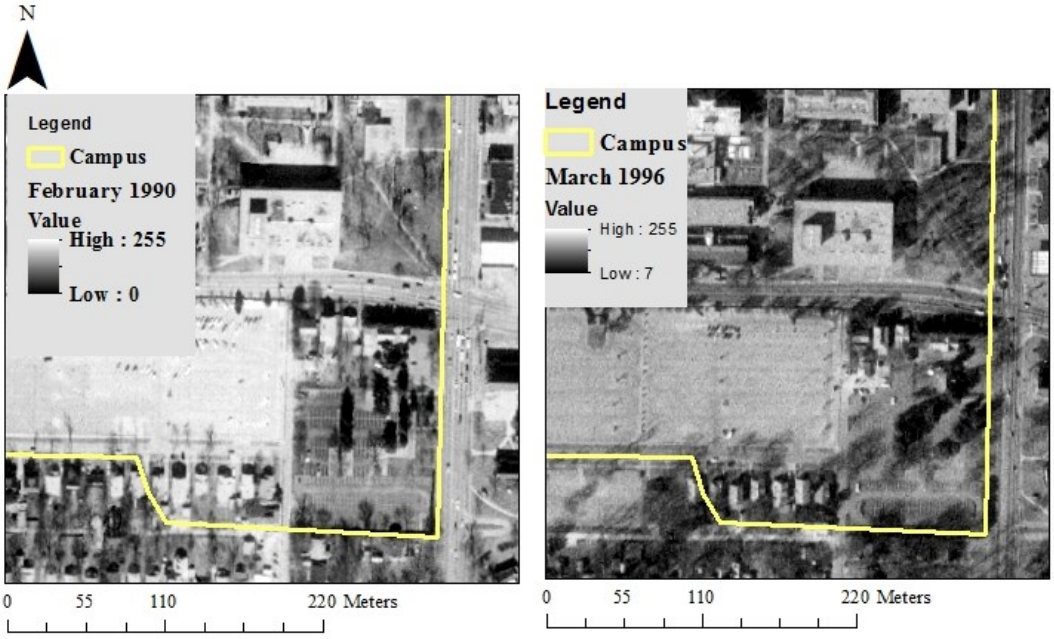

Fig. 7. Aerial photographs displaying basin features from the years 1990 (left) and 1996 (right)

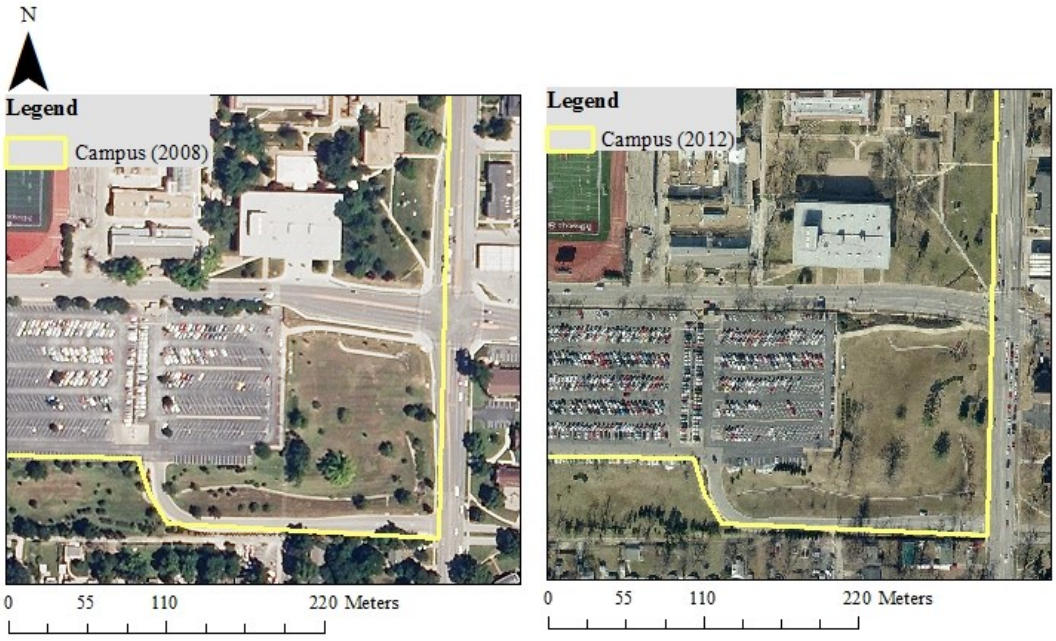

Fig. 8. Aerial photos of basin after construction from 2008 (left) and 2012 (right).

METHODS

Field Methods

Bottom sediment samples were collected from sediment deposits along the drainage network throughout the basin, including the trickle channels, adjacent basin surfaces, and the active sediment deposits near inlets and outlets. Sample jars and containers were provided by the Peoria Disposal Company (PDC) Laboratories, located in Springfield, Missouri. Specific locations were selected, based on the inflow of the water and topography of the basin (Pies et al., 2007; Fischer et al., 2003). Samples were taken in November of 2015 and September of 2016. The 2016 samples were collected approximately one year later to maintain seasonal consistency. Sampling occurred at two separate times to first evaluate the 2015 PAH concentrations and determine appropriate coring locations.

November 2015, Sediment Collection. Approximately 5 cm of surface sediment was collected at 30 sampling locations to represent the spatial distribution and deposition of PAHs within each location of the basin (Figure 9) (Wang et al., 2002). Each sample was collected with the use of a trowel. They were each placed in a separate glass jar and labeled accordingly. A GPS coordinate point was taken at each sampling location. Once all sediment samples were collected, they were returned to the PDC Laboratory for the evaluation of PAH concentrations.

September 2016, Sediment Collection. Twenty-four additional samples were collected, including both core, surface, and loose sediment (road-side samples) accumulated along the curbs of Grand Street and National Avenue (Figure 10). The core

samples included three sediment cores taken from the same study basin, approximately 30-35 centimeters in length. These samples were collected using a split-core sampler. Once the sediment core had been extracted from the ground, it was separated into sections based on varying characteristics of the soil layers. An additional sediment core was taken next to the original core collected. This secondary core was also separated into sections and placed in freezer bags. These samples were listed as the "duplicate core" samples and they were taken back to the MSU laboratory. The duplicate core samples were not tested for PAH concentrations, but were analyzed for all other sediment properties. The 2016 core locations were altered from the initial selected regions due to the removal of sediment from basin channels, resulting in the disturbance of the basin. The surface and roadside samples were collected along Grand Street and National Avenue, locations leading into storm drainage lines or strong runoff regions on the MSU campus, and one sample was collected at the edge of the coal-tar parking lot next to the detention basin.

Sediment Sampling. Throughout the two sampling periods, three separate types of sediment sampling occurred. These included: Bottom and channel sediment, core sampling, and catchments and road sampling (Table 1). The 2015 sediment sampling included the bottom and channel sediment collection (Figure 9). This included the basin soil and trickle channel sediment surface sampling. These specific samples included collecting the uppermost 0-10 cm of sediment using a hand trowel (Andronikov et al. 2000; Xiao et al., 2011). The core sampling took place in 2016. Sediment cores collected were 30-35 cm in depth. Correspondingly in the 2016 sampling event, six sediment samples were collected from locations on campus and adjacent roads in the contributing

watershed. These remaining six selected were collected within the delineated watershed contributing to the detention basin (Figure 10).

Table 1. Number and type of samples collected during two sampling periods

Sample Type	2015	2016	Total
Surface	30	0	30
Core	0	18	18
Roadside	0	6	6
Duplicate Core	0	15	15

Topographic Surveys. During the 2015 field sampling, transects were taken at each sampling location using the auto-level, stadia rod, and a 100 meter tape (Appendix E) to evaluate the changes in elevation and topography. Samples were mainly collected along the survey transect line to provide accurate elevation measurements for each sampling location. The distance of the samples from the transect line were recorded along with the elevation of each sample location.

Fig. 9. Locations of 2015 surface samples

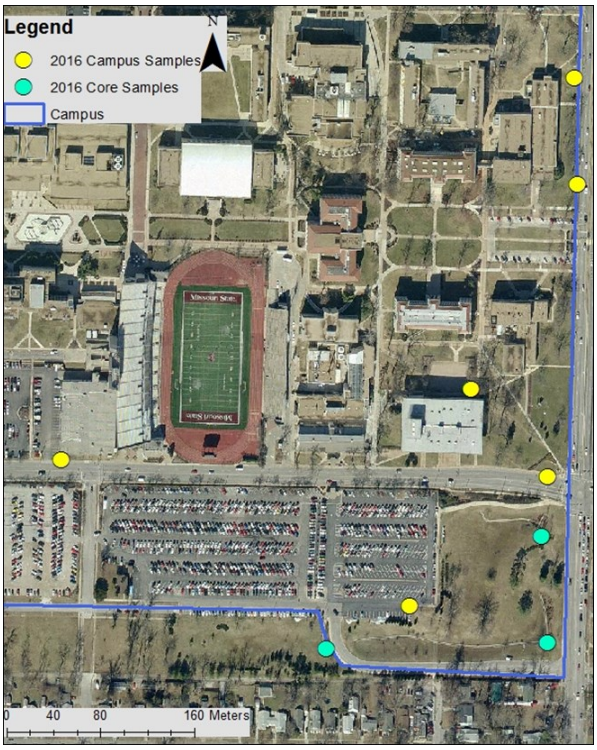

Fig. 10. 2016 sediment samples collected on campus and core samples

Laboratory Analysis

To understand the extent of contamination within the selected basin, different laboratory methods were used to begin the sediment analysis. Standards, blanks, and duplicate samples were processed throughout all laboratory tests following individual OEWRI SOPs. The validity and quality of results were determined through relative percent difference (RPD) and quality assurance and quality control (QA/QC) between duplicates and standards (New Jersey Department of Environmental Protection, 2014).

Sample Preparation. The sediment samples collected were first placed in glass jars and transported to PDC Laboratories in order to determine the PAH concentrations. After the samples were returned to MSU, samples were placed in drying ovens at 60^{o} Celsius for approximately 24 hours (Pavlowsky, 2013). After samples were removed from the drying ovens, sediment samples were then weighed in the glass jar without the lid. Jar weight was tared to view only the sample weight. Once samples were weighed, sediment was sieved to < 2 mm. After the completion of sieving, all samples were placed in specific XRF bags and labeled accordingly by sample name and date collected. Preparation methods were completed following the designated OEWRI SOPs.

Organic Matter Loss on Ignition (OM-LOI). The methods followed were generated by the SSSA methods of soil science. All samples were placed in laboratory ovens at 105^{o} Celsius for four hours. Samples were then placed in a corresponding oven at 600^{o} Celsius for eight hours (OEWRI SOP). Standard calculations may be seen in the OEWRI SOP.

Sediment and Soil pH. The pH values of selected samples were determined to understand the acidity levels and potential effect on pollutant mobility of the sediment

samples collected within the basin. Following the OEWRI designed SOP (http://oewri.missouristate.edu/assets/OEWRI/OEWRI_SOP_003_pH_9-30-15_.pdf), the pH values of a select 11 samples were tested using the pHep pH analysis meter. These samples were taken from the most recent 2016 sediment samples. The 2016 samples were used in order to observe the acidity levels as sample's depth increased. Another stipulation influencing the sample selection was the amount of sediment remaining after all laboratory tests had been completed. The pH meter was calibrated with pH 4.0 and 7.0 pH buffers (OEWRI SOP). Two duplicates and a DI blank were run throughout the analysis. Twenty grams of sediment were added to 20 mL of DI water in a 250 mL beaker and stirred with a glass rod approximately every 20 minutes for six hours.

Laser Diffraction Particle Size Analyzer (LS 13 320). The laser diffraction particle size analyzer was used to determine the different grain sizes within each individual sample (Di Stefano et al., 2010). This test was performed using the laboratory instrument LS 13 320 following the OEWRI SOP for this laboratory instrument (http://oewri.missouristate.edu/assets/OEWRI/Particle_Sizer_R01_Final_.pdf). This process was performed five times with two duplicates per batch. Both the 2016 PAH analyzed and duplicate core samples were tested for grain-size analysis. Quality assurance and check (QA/QC) permitted a (±) 20% error for data. All duplicate RPDs were averaged to understand the overall percent error for the total samples (OEWRI SOP). Overall percent error for samples (n=69) run were as follows: Sand, 13.6%; silt, -14.1%; and clay, -11.5% error. All determined values were below the QA/QC limit of (±) 20% (Appendix C-2).

Gas Chromatography-Mass Spectrometry (GC/MS) Method 8270. Sediment and soil samples were analyzed for PAH concentration by PDC laboratories (1805 W Sunset St, Springfield, MO 65807). An Agilent 7890A instrument and GC/MS Method 8270 was used to determine the concentration amounts of each individual types of PAHs within each sample. GC/MS is used to separate volatile and organic compounds within a given mixture or solution and determine the molecular composition of each sample (Philips Innovation Services, 2013). Thus providing the values of individual PAHs within each sample tested.

Once raw data was received from PDC laboratories, the total concentration of each sample was determined by combining the concentrations of the EPA_{16} standard PAHs. PAH analysis is based upon the EPA_{16}, which selects 16 specific PAHs to use in contamination comparison (Khadar et al., 2010; Pavlowsky, 2013; Irwin et al., 1997). The select PAH types were added together to conclude the final concentration for each sample. Any individual PAH analyses that received a "less-than" value, indicating that the sample value was below detection limit (< DL) were given a concentration value assumed to be half of the detection limit (i.e. A value of < 2,200 yields 2,200/2, resulting in a value of 1,100 to be added to the concentration total).

X-Ray Fluorescence Analysis Method 6200. XRF method 6200, following the OEWRI provided SOP, was used to analyze the sample for elemental concentrations (Gowd et al., 2010; Howari et al., 2000). The elements of focus were chosen to be lead (Pb), zinc (Zn), copper (Cu), iron (Fe), manganese (Mn), and calcium (Ca). Samples were analyzed in two batches (2015 and 2016 samples). Each batch had two duplicates and two standards, which were averaged for a single precision and accuracy value (OEWRI

SOP). The overall determined precision (n=69) for Pb was 28.4%, Zn was 3.6%, Cu was 2.6%, Fe was 3.8%, Mn was 7.6%, and Ca was 13% (Appendix B-5). Precision should be within (±) 20% of the duplicate (http://oewri.missouristate.edu/assets/OEWRI/XRF.pdf). The average precision for all elements were below the (±) 20% level, with the exception of Pb which was 8% higher than QC limit (OEWRI SOP). The probable cause of the high RPD of Pb was that the duplicate sample 38A had increased amounts of sand (>70%) (Appendix B-3). Sand-sized grains have the potential to disrupt XRF readings and result in skewed results (OEWRI SOP). However, the overall accuracy (n=69) determined for Pb was 1.6%, Zn was -5.3%, Cu was 0.8%, Fe was -3.4%, Mn was 9.9%, and Ca was -3.7% (Appendix B-4). All accuracy values determined were within the (±) 20% QA/QC limit (Jasperoid Standard Concentration; OEWRI SOP).

Cesium-137. Cesium-137 (Cs-137) was calculated as a method to understand the age of the basin and a generalized understanding of how long the contaminants have been accumulating (Ritchie and McHenry, 1990). Cs-137 has no natural source of introduction into the environment, and is only produced through nuclear fission primarily induced by nuclear weapons testing (Ritchie and McHenry, 1990). The first introduction of Cs-137 into the environment was in the year 1952 and the peak concentration occurred in 1963-1964 (Ritchie and McHenry, 1990; USGS, 2016). Following the OEWRI SOP, each of the duplicate core samples were transferred from the XRF bags to containers specified for the gamma spectrometer. Samples were then analyzed for the concentration of Cesium-137 located within the sample. Samples were tested using the Gamma spectrometer. A total of fourteen samples and two duplicate samples were analyzed by the gamma spectrometer. All core samples were analyzed except for one, 38B. Sample 38B had an

inadequate amount of sediment remaining to provide an accurate result reading. Units were altered from Curie (uCi/Unit) to Becquerel (Bq/kg), in order to continue analyses. To convert the units from Curie to Becquerel, the equation

$$uCi/kg * 37{,}000$$

was used (OEWRI SOP). This was performed for both uncertainty and activity values.

ArcGIS

ArcGIS was used as a method to view spatial and topographic relationships throughout the data (Kooistra et al., 2001). An initial map generated included all detention basins on the campus, drains, pipelines, campus buildings, roads, and parking lots. All data used for this map was generated by the Missouri State University Facilities Management. This data was extracted from the OEWRI server and entered into ArcMap. Once this general map was created, a digital elevation model (DEM) was added to see any significant topography. The DEM data was found on the OEWRI server database.

The drainage network and flow direction were provided by MSU and observations by the author. Observations during and after storms assisted in the knowledge of the campus runoff movement.

DEM and LiDAR Analysis. Supplied by the OEWRI server, a one-meter LiDAR and DEM of the detention basin and campus was added to a blank map. This bare-earth DEM was the standard DEM used for all terrain analysis of the detention basin. The OEWRI server also provided the LiDAR and aerial imagery of Springfield, MO from the year of 2012. Both datasets were used as the basis for the following GIS procedures. After both 2015 and 2016 sampling occurred, the GPS coordinates were taken at each

sample location using a Trimble and corresponding PAH concentrations were added to the GIS map.

Watershed Delineation and Elevation. The local watershed within or adjacent to the basin was delineated as a way of understanding the watershed behavior. This was performed by using the watershed tool in ArcGIS. The resulting delineated watershed feeding the basin was further separated into three categories: West (W), Northwest (NW), and North (N). The separation of the watershed made it possible to calculate the total amount of the basin being influenced by different sources (Vittala et al., 2008; Comair et al., 2012). Once the watershed had been identified, the area of the watershed was calculated. The area calculations were performed in ArcGIS 10.4 using the Calculate Geometry tool.

To determine the elevation in meters above sea level, the Point to Value Spatial Statistics tool in ArcGIS was used. This method compared the sampling GPS point to the location on the base DEM. By doing so, it calculated a list of elevation values for each sampling location.

Statistical Analysis

To observe correlations between the differing factors, statistical methods were required. The statistical analysis portion of this study was based on 30-54 sample values. Two programs were used to complete statistical analysis: IBM SPSS Statistics program version 22 and Microsoft Office Excel, 2013. Statistical testing and correlations incorporated all 2015 and 2016 values, which have been analyzed for PAH concentration.

In order to visually observe any correlations between the samples, GIS was utilized for additional statistical testing.

IBM-SPSS. Sample data was entered into the IBM-SPSS to develop regression models using multiple variables (Rogerson, 2010). The regression model chosen for analysis was a multivariate, linear regression model. Pearsons R values were used for statistical comparison throughout data. This was used as a method to observe any influences on PAH concentrations throughout the basin or among other existing variables. This regression model assumed that there was no multicollinearity between independent variables (Rogerson, 2010).

Excel Computer Program. All field and laboratory data and results were entered into Excel datasheets. IBM-SPSS results were also added into Excel for further data analysis and representation.

RESULTS AND DISCUSSION

This chapter presents the results and analysis of PAH concentrations in channel, bottom, core, and catchment from sediments collected from the stormwater basin system. Sixty-nine samples were evaluated including, 30 basin, 18 core, 5 road/campus, 1 edge of parking lot, and 15 duplicate core samples. Fifty-four samples were evaluated for PAH concentration including, 30 basin, 18 core, five road/campus, and one edge-of parking lot samples. Throughout the duration of this study, 54 PAH-analyzed samples were collected. However, for sub-basin analysis, there were limited numbers of samples available for statistical analysis for each sub-basin. Though definite trends were observed, the small numbers of samples collected did not allow for statistically significant conclusions. Samples were not uniformly distributed throughout the basin, but focused primarily at inlets, outlets, and trickle channels. This prohibited the complete analysis of sediment distribution throughout the basin.

Watershed Analysis and Land Use

The drainage area of the stormwater basin is 0.22 km^2. Within the total drainage area, the permeable surfaces covered 46.8% of the total watershed. The smallest contributor was roads with 11.4% (Table 2). The watershed areas drain into the stormwater basin and encompass a portion of Grand Street, National Avenue, parking lots 22 and 24, and the eastern portion of the MSU campus. The basin is separated into three regions (Table 2). The basin receives drainage from three sub-areas: West, Northwest, and North (Figure 11).

The West sub-watershed influenced approximately 0.043 km^2 in area and 20% of the central retention basin. The majority of the West sub-watershed was covered by the coal-tar lots 22 and 24, which contributed approximately 70% of the West sub-watershed. The Northwest portion, receiving the main runoff from a portion of campus and Grand Street, is roughly 0.076 km^2 in area and influences approximately 56% of the central retention basin. The North portion, which receives runoff from the corner of Grand Street and National Avenue, is approximately 0.102 km^2 and contributes the remaining 23% of the primary, central basin (Figure 11).

Table. 2. The square kilometers and percent contribution from land use in the watershed elements

Watershed Areas	Permeable Surface (km^2)	Parking lots (km^2)	Roads (km^2)	Buildings (km^2)	Total Area (km^2)
Total (km^2)	0.103	0.048	0.025	0.045	0.221
%	46.8	21.6	11.4	20.3	(100%)
West (km^2)	0.010	0.030	0.003	0.000	0.043
%	4.51	13.62	1.45	0.06	(19.5%)
Northwest (km^2)	0.039	0.001	0.010	0.026	0.076
%	17.93	0.38	4.36	11.76	(34.4%)
North (km^2)	0.054	0.017	0.012	0.019	0.102
%	24.33	7.58	5.55	8.47	(46.1%)

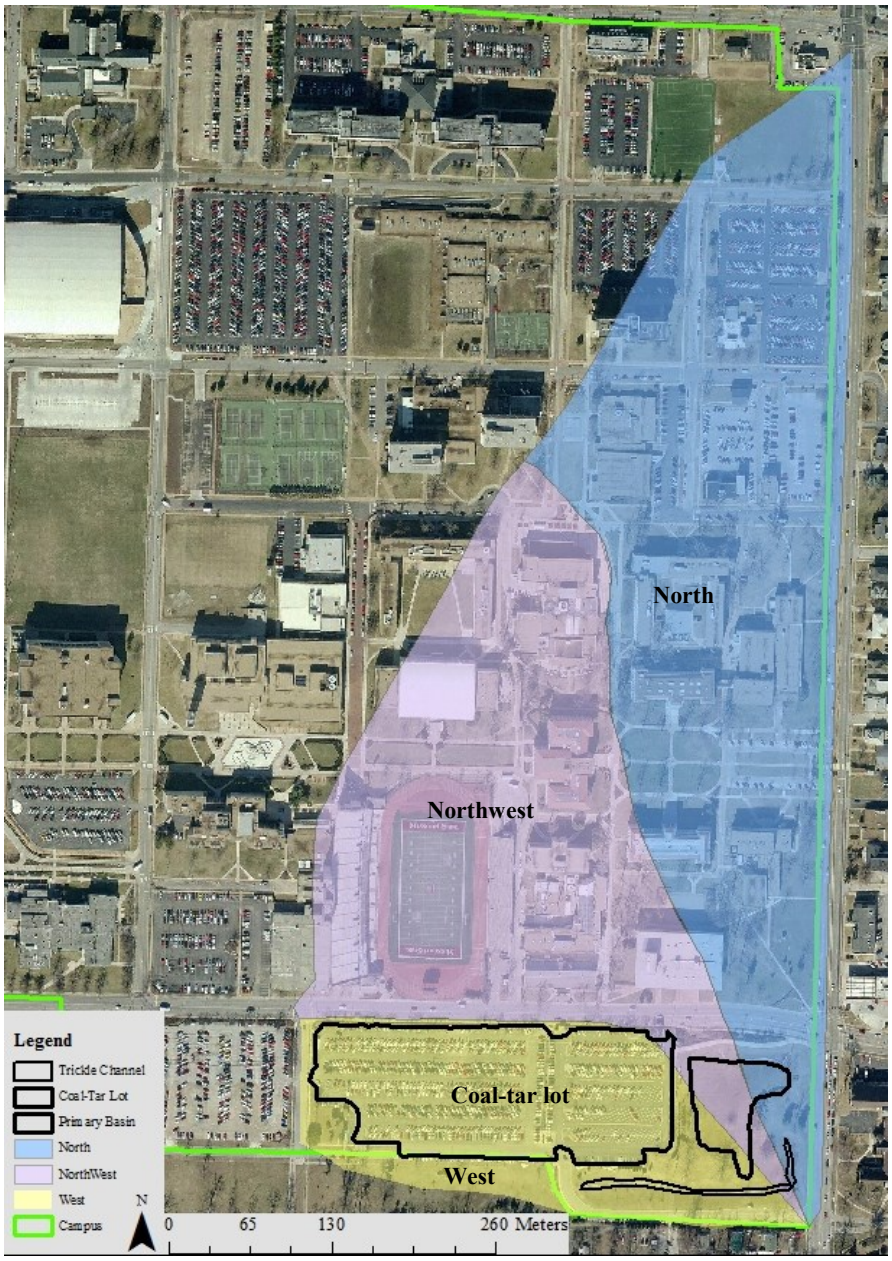

Fig. 11. The segmented watershed feeding the detention basin

Basin Sediment Analysis

The primary results of the basin analysis include PAH concentrations (µg/kg), metal concentrations (ppm), grain size analysis, and OM-LOI.

PAH Contamination. Published toxicity limits indicate that sediment-PAH_{16} concentrations below 1,610 μg/kg are considered non-toxic. Alternatively, concentration levels that are above 22,800 μg/kg are considered to be toxic and harmful to sediment-dwelling organisms (MacDonald et al., 2000). Sample values show that of the 54 samples evaluated, 65% are above the toxicity level and are considered to be harmful to the environment (Appendix A-1). The remaining 35% were above the non-toxic limit, but did not exceed the 22,800 μg/kg threshold. Samples were separated into two groups: basin and channel samples (Figures 13a-13b). Basin samples were soil samples collected from grassy areas adjacent and distant from channel (Figure 13a). Channel samples were collected in trickle channels, inlets, or outlet regions (Figure 13b). It was found that channel samples contained higher concentrations compared to basin soil samples, disregarding the south sub-basin since (no channel samples were collected within the south sub-basin) (Figure 14). All channel samples contained total PAHs above 22,800 μg/kg (Table 3). The basin soil samples showed the lowest percentage of samples above the toxicity level, but all samples were above the threshold limit (Table 3). Two-thirds of core and road samples were above the toxic level (Table 3).

The 2015 basin samples (n=30) were separated into four sub-basins based on the inlets and outlets of the basin as well as flow paths. These sub-basins included: West inlet, South, Central outlet, and Central sub-basins (Figure 12). The West inlet sub-basin incorporated the coal-tar sealed parking lot inlet region. The Central outlet sub-basin included the outlet region in the eastern corner of the basin. The South sub-basin was the trickle channel between the West inlet and the Central outlet. The Central sub-basin included the northern two inlets and a portion of the northern primary basin.

Table 3. The percentage of each sample type for a given toxicity limit.

	Channel	Basin	Core	Roads	Limit (µg/kg)
n	10	20	18	6	N/A
Not toxic	0%	0%	0%	0%	< 1,610
Threshold	0%	55%	33%	33%	1,610-22,800
Toxic	100%	45%	67%	67%	> 22,800

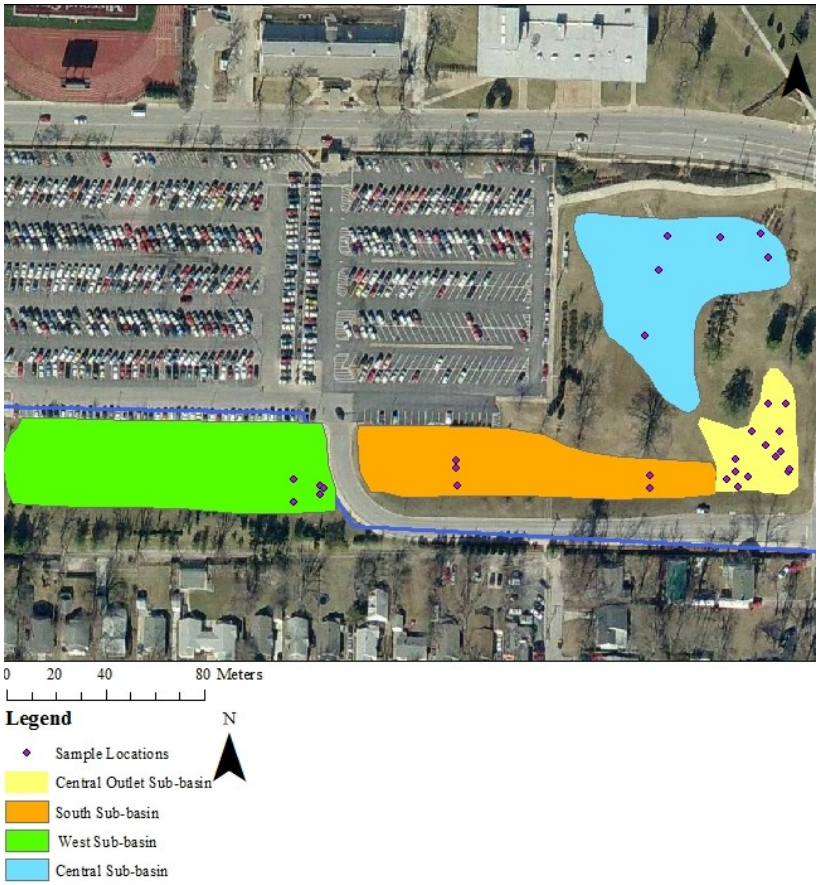

Fig. 12. Sub-basins in the detention basin

The sub-basin with the highest PAH concentration was the Central outlet, with a maximum concentration of 712,500 µg/kg. The sub-basin with the lowest concentration was the South, with a maximum value of 41,100 µg/kg (Table 4).

Table 4. PAH_{16} concentrations for each sample type and location

Sample type		West (µg/kg)	South (µg/kg)	Central Outlet (µg/kg)	Central (µg/kg)	Road-side (µg/kg)
Channel	n	2	-	6	2	-
	Minimum	258,150	-	94,200	90,200	
	Median	397,700	-	198,100	145,300	
	Maximum	537,250	-	712,500	200,400	
Basin	n	3	5	8	4	-
	Minimum	9,855	3,280	5,445	3,485	
	Median	15,235	3,520	46,325	26,228	
	Maximum	93,400	41,100	80,500	43,300	
Core	n	7	-	5	6	-
	Minimum	3,200	-	12,950	21,670	
	Median	9,250	-	61,150	42,790	
	Maximum	206,300	-	79,450	220,600	
Roads	n	-	-	-	-	6
	Minimum	-	-	-	-	9,940
	Median	-	-	-	-	50,575
	Maximum	-	-	-	-	534,650

A

B

Fig. 13. Basin soil sample collected (A) and channel sediment sample collected (B)

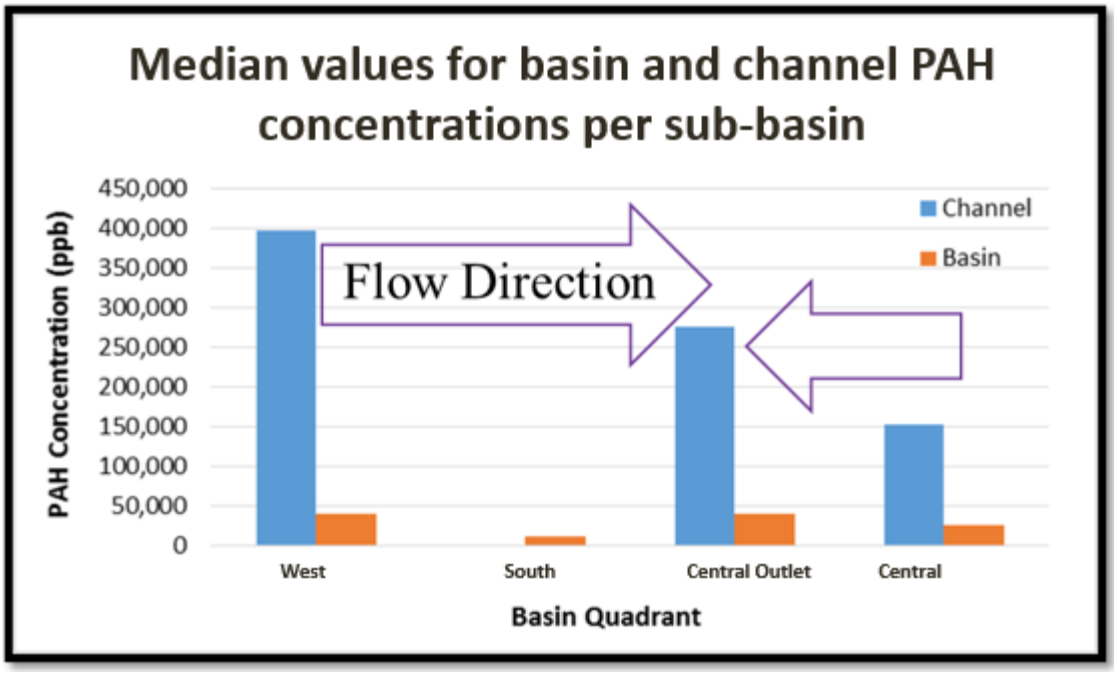

Fig. 14. Channel and basin total PAH_{16} concentrations of each sub-basin

2015 Sub-basin Metal Concentration. The total basin heavy metal concentrations were also separated into four sub-basins. The sub-basin values were based on the original 2015 samples, which included 30 samples (Table 5) (Appendix B-1 - B-9).

Table 5. Sub-basin sediment-metal concentration

Sample Location		n	Pb (ppm)	Zn (ppm)	Cu (ppm)	Fe (ppm)	Mn (ppm)	Ca (ppm)
West		5						
	Minimum		29	56	10	16,274	207	3,435
	Median		64	122	10	18,163	545	25,391
	Maximum		78	244	10	28,776	792	113,898
South		5						
	Minimum		35	53	< DL	19,572	433	2,327
	Median		47	76	< DL	21,066	616	3,501
	Maximum		65	115	< DL	23,597	664	11,063
Central Outlet		14						
	Minimum		41	78	11	17,145	94	2,979
	Median		75	430	80	20,396	416	86,498
	Maximum		135	673	169	31,098	727	245,052
Central		6						
	Minimum		53	174	14	18,892	320	14,032
	Median		78	231	21	21,194	421	89,640
	Maximum		107	1,019	279	29,900	484	197,374

The highest median concentrations of each of the individual metals was found to be in the Central outlet (n=14). The lowest total concentration of each individual metal was located in the South sub-basin (n=5), except for Mn and Fe (Figure 15). The highest levels of Pb within the Central Outlet sub-basin had a maximum concentration of 135

ppm and total concentration of 1,137 ppm (Figure 15). The determined value of 135 ppm is above the toxicity level of 128 mg/kg (Macdonald et al., 2000; Agency for Toxic Substances and Disease Registry, 2007). No other individual Pb values were found to exceed the designated toxicity level, but two samples did fall below the non-toxic threshold of 35.8 mg/kg (Macdonald et al., 2000). The greatest Zn values had a maximum value of 673 ppm and a total concentration of 5,973 ppm. Total Cu concentration in the SE sub-basin was concentration of 842 ppm. The greatest individual Cu concentration was found in the Central sub-basin (n=6), reaching a max value of 279 ppm. Copper values were significantly lower in the West inlet (n=5) and South sub-basins, providing a maximum value of 10 ppm in the West inlet sub-basin and value below detection limit within the South sub-basin. The Fe levels were significantly higher in the Central outlet sub-basin with a total concentration of 317,787 ppm and maximum individual sample value of 31,098 ppm also located in the Central outlet sub-basin. The West inlet sub-basin was found to have the lowest Fe value, with a total concentration of 102,826 ppm. The maximum individual sample value for Mn was located in the West inlet sub-basin, reaching 792 ppm. The highest total concentration of Mn was found in the SE sub-basin reaching 6,461. Calcium was shown to have the highest individual value, totaling 245,052 ppm in the SE sub-basin and total concentration of 1,511,904 ppm in the SE sub-basin. The lowest concentration values for Ca were found in the South sub-basin, with an individual value of 11,063 ppm and total concentration of 188,563 ppm (Figure 15). Sub-basin samples were averaged to observe the overall contamination per region.

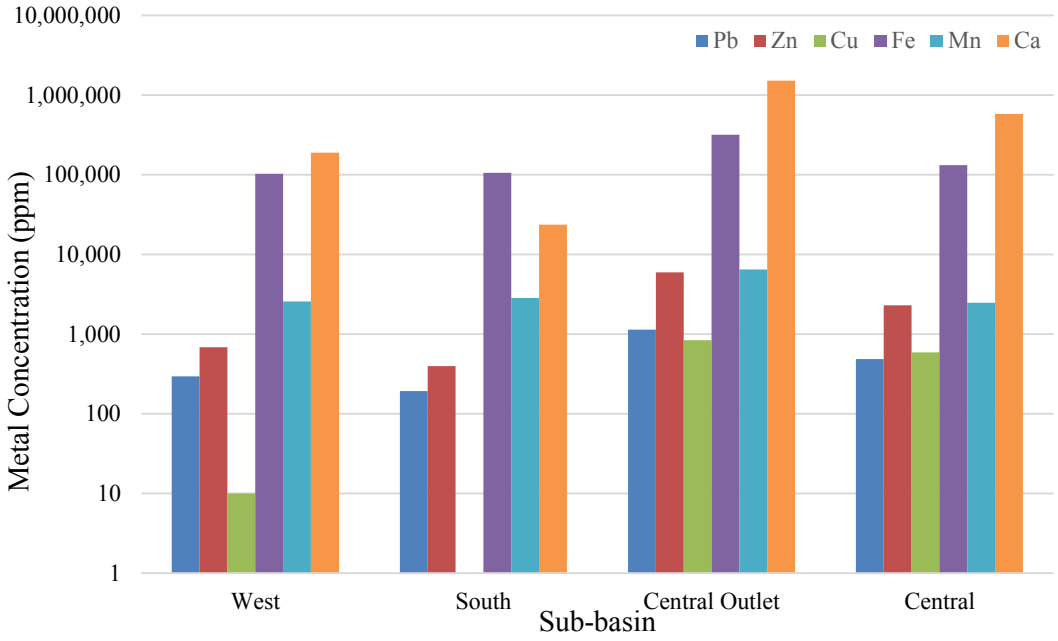

Fig. 15. Metal concentration by sub-basin

Grain Size Analysis. Percent sand was found to have the maximum percentage for all sub-basins excluding the south sub-basin (Table 6) (Appendix C-1). The South sub-basin showed that silt was the maximum percentage of substrate, whereas sand was the lowest percentage of the substrate type (Table 6). The West inlet and Central outlet showed similar behaviors with grainsize percentages, with a maximum sand percentage of approximately 85% (Table 6). Clay, however showed a higher percentage in the Central outlet with 37% compared to the West inlet clay contribution of 21%.

Sand concentration was significantly higher in channel samples compared to basin soil samples (Table 6). Silt and clay were higher in basin samples compared to channel sediment samples.

Table 6. Grain size concentrations for each sub-basin

Location	n	Sand (%)		Silt (%)		Clay (%)	
		Channel	Basin	Channel	Basin	Channel	Basin
West	5	(n=2)	(n=3)	(n=2)	(n=3)	(n=2)	(n=3)
Maximum		85.4	11.4	30.7	76.1	10.3	21.0
Median		72.1	9.5	20.7	69.6	7.2	20.9
Minimum		58.9	4.1	10.7	67.6	4.0	19.9
South	5	(n=0)	(n=5)	(n=0)	(n=5)	(n=0)	(n=5)
Maximum		-	11.0	-	70.7	-	22.1
Median		-	9.4	-	69.3	-	20.8
Minimum		-	8.3	-	68.3	-	20.7
Central Outlet	14	(n=6)	(n=8)	(n=6)	(n=8)	(n=6)	(n=8)
Maximum		85.0	22.2	58.6	72.0	16.1	37.4
Median		73.1	11.3	20.4	67.5	6.5	21.2
Minimum		25.3	7.0	10.5	51.8	4.3	17.4
Central	6	(n=2)	(n=4)	(n=2)	(n=4)	(n=2)	(n=4)
Maximum		75.1	73.1	26.0	73.7	8.6	22.5
Median		70.3	12.2	22.5	67.3	7.2	19.2
Minimum		65.5	6.4	19.1	20.8	5.8	6.1

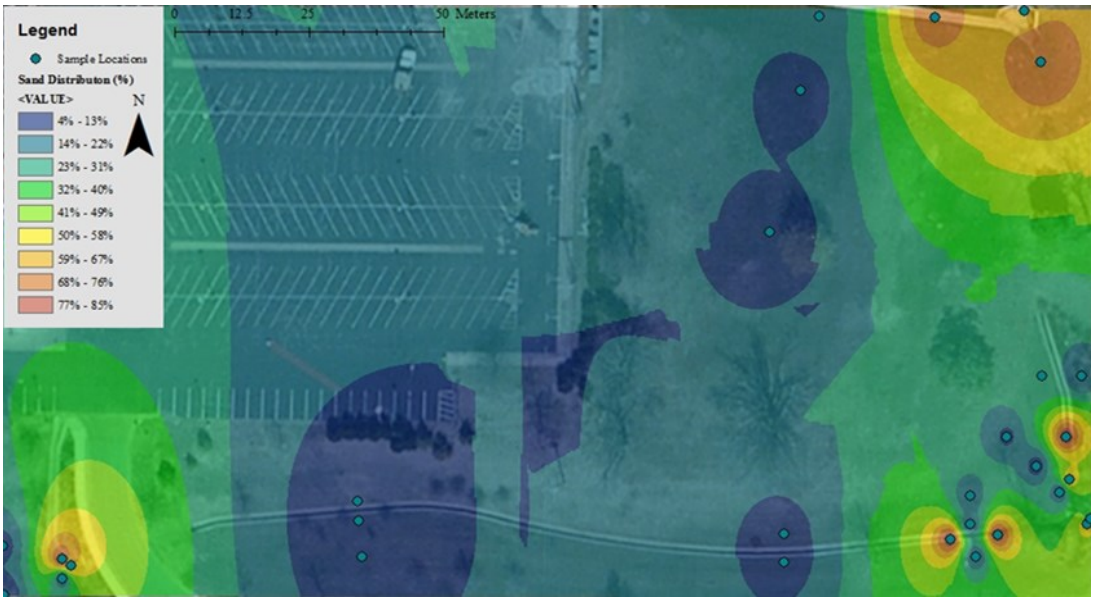

Fig. 16. Percent sand distribution throughout the basin (n=30)

The areas closest to the inlets and outlet had highest percentages of sand compared to the basin soil samples, which were higher in silt and clay (Figure 16). However, the Central outlet had the highest percentage of clay, but receives runoff contribution from all regions of the basin.

There was an inverse relationship between sand and silt/clay. Sand content generally had a positive relationship with the increase in PAH concentration, whereas silt and clay had a negative correlation (Figure 17). The correlations between PAH contamination and sand may indicate source contamination, rather than substrate preference. Following the OEWRI SOP (http://oewri.missouristate.edu/assets/OEWRI/Particle_Sizer_R01_Final_.pdf), total percent error calculated for all samples and sand standards was found to be below the (±) 20% limit (Appendix C-2 and C-3).

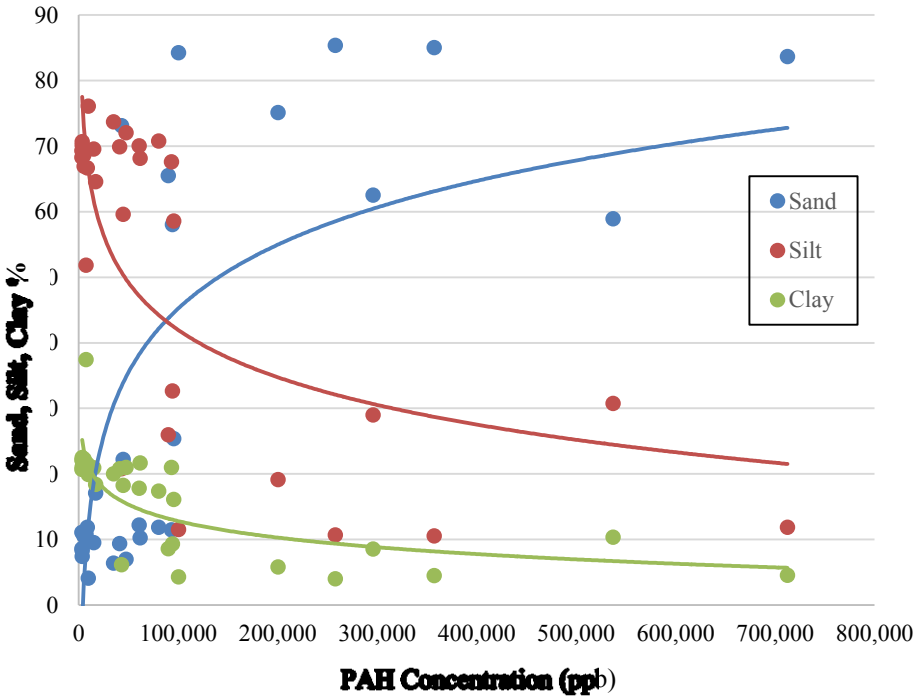

Fig. 17. Relationship of grain size to PAH concentrations

The method selected for grainsize analysis (laser diffraction particle size analysis) is often not the standard measurement used for grain size analysis. The sieve-hydrometer is most commonly used for grainsize distribution analysis (Di Stefano et al., 2010). The laser diffraction method has been found, in certain cases, to inaccurately interpret the sand and clay percentages, overestimating the sand percent and underestimating the clay percentages (Di Stefano et al., 2010). The QA/QC methods used for the laser diffraction particle size analysis are unable to accommodate samples which have high sand content. To account for this, the overall average RPD was recorded for all duplicates (Appendix C-2 and C-3).

OM-LOI. The frequency distribution of OM-LOI for each sub-basin was calculated to determine any influence or patterns found in relation to contaminants and

organic matter concentrations (Syroventik et al., 2007; Oakley et al., 1981). Organic matter may increase the mobility of contaminant particles, particularly metals, so it is assumed that regions with higher organic percentages may result in regions of higher contamination concentration (Syroventik et al., 2007). Organic matter is also considered a strong adsorbent for PAH particles if the organic matter is found in high concentration (Yang et al., 2008; Srogi, 2007).

OM-LOI results (Appendix D-1) showed similar behavior as the metal concentrations. OM-LOI values were highest in the basin soil samples in the Central outlet and Central sub-basins and lowest in the channel sediment in the South and West sub-basins (Table 7).

Table 7. LOI for each sub-basin

Sample Location	n	LOI	
West	5	Channel (n=2)	Basin (n=3)
Maximum		5.7	10.6
Median		5.6	10.2
Minimum		5.5	6.8
South	5	Channel (n=0)	Basin (n=5)
Maximum		-	12.0
Median		-	10.1
Minimum		-	8.4
Central Outlet	14	Channel (n=6)	Basin (n=8)
Maximum		23.8	14.0
Median		10.6	11.5
Minimum		5.7	10.3
Central	6	Channel (n=2)	Basin (n=4)
Maximum		12.7	10.2
Median		11.2	10.1
Minimum		9.7	8.0

Spatial Distribution of PAH and Metal Sources in the Basin. The spatial distribution patterns observed throughout this study have shown significant patterns with PAH contamination in relation to location and elevation. Contamination decreases as it increases in distance from inlets and outlet locations (Motelay-Massei et al., 2004; Feng et al., 2007). As seen in Figure 18, the regions of highest concentrations are found near the runoff inlets and outlet regions. PAH contamination had the highest concentrations in the SW inlet and SE outlet. The West inlet was supplied by a coal-tar sealed parking lot and the SE outlet received runoff from the entire basin (Figures 18a-18b). Locations with the lowest concentrations showed to be the central basin, furthest from the inlet regions.

A

B

Fig. 18. Trickle channel leading to Central outlet (A). Trickle channel located in West sub-basin (B)

As elevation increased, the PAH concentration sequentially decreased (Appendix A-7) (Guo, 1997). However, results showed that at the elevation of 396.4 m, residing in the SW outlet, a concentration spike occurred (Figure 20). The samples found to increase, despite elevation, were channel samples. This suggests that elevation has a strong influence on contamination levels, but different sources and locations may have increased exposure to PAHs (Guo, 1997).

Metal concentrations showed similar trends as PAHs, concentrating near inlets and outlet regions of the basin (Figure 21). The Central sub-basin generally had low levels of metal contamination except for Pb. Lead values were highly concentrated in the Central outlet and Central sub-basin; all other metals were generally low concentrations throughout the Central sub-basin (Figure 21). Copper and Zn values were lowest near the West inlet sub-basin (near the coal-tar sealed parking lot) and highest in the northern inlet and Central outlet. Manganese was most concentrated along the trickle channel ranging from the West inlet, through the South sub-basin, to the Central outlet. Calcium was found primarily in the inlets and outlet regions, but low in the South and Central sub-basins (Figure 21).

Local sedimentation patterns appear to have the strongest influence on metal distribution. The highest concentrations of metals were typically found near inlets and outlet regions of the basin with lower values with increased distance from the inlet sources (Motelay-Massei et al., 2004). However, metal type varied by location, which suggests that additional sources may be contributing to metal contamination (Figure 21).

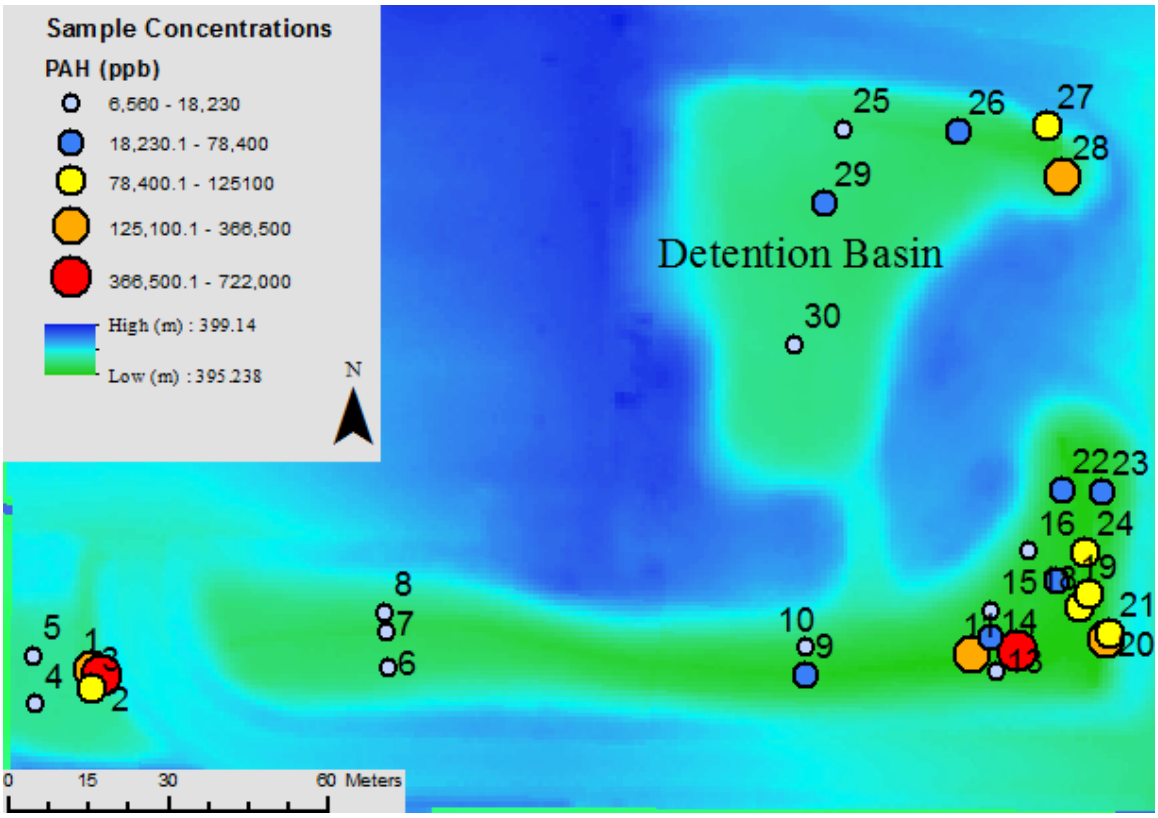

Fig. 19. Distribution of sediment-PAH concentrations of basin sampling locations. Detention basin with the sampling locations and PAH concentrations

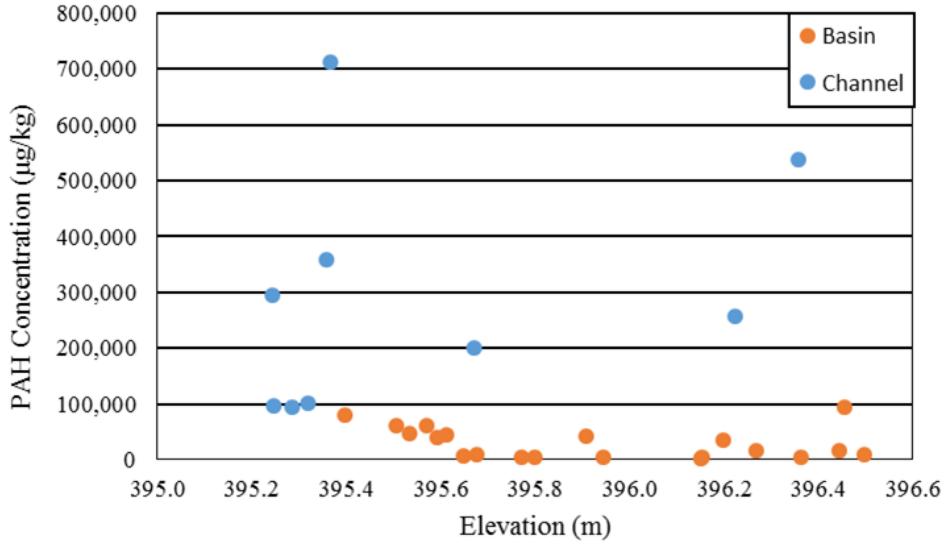

Fig. 20. PAH concentration changes in response to elevation

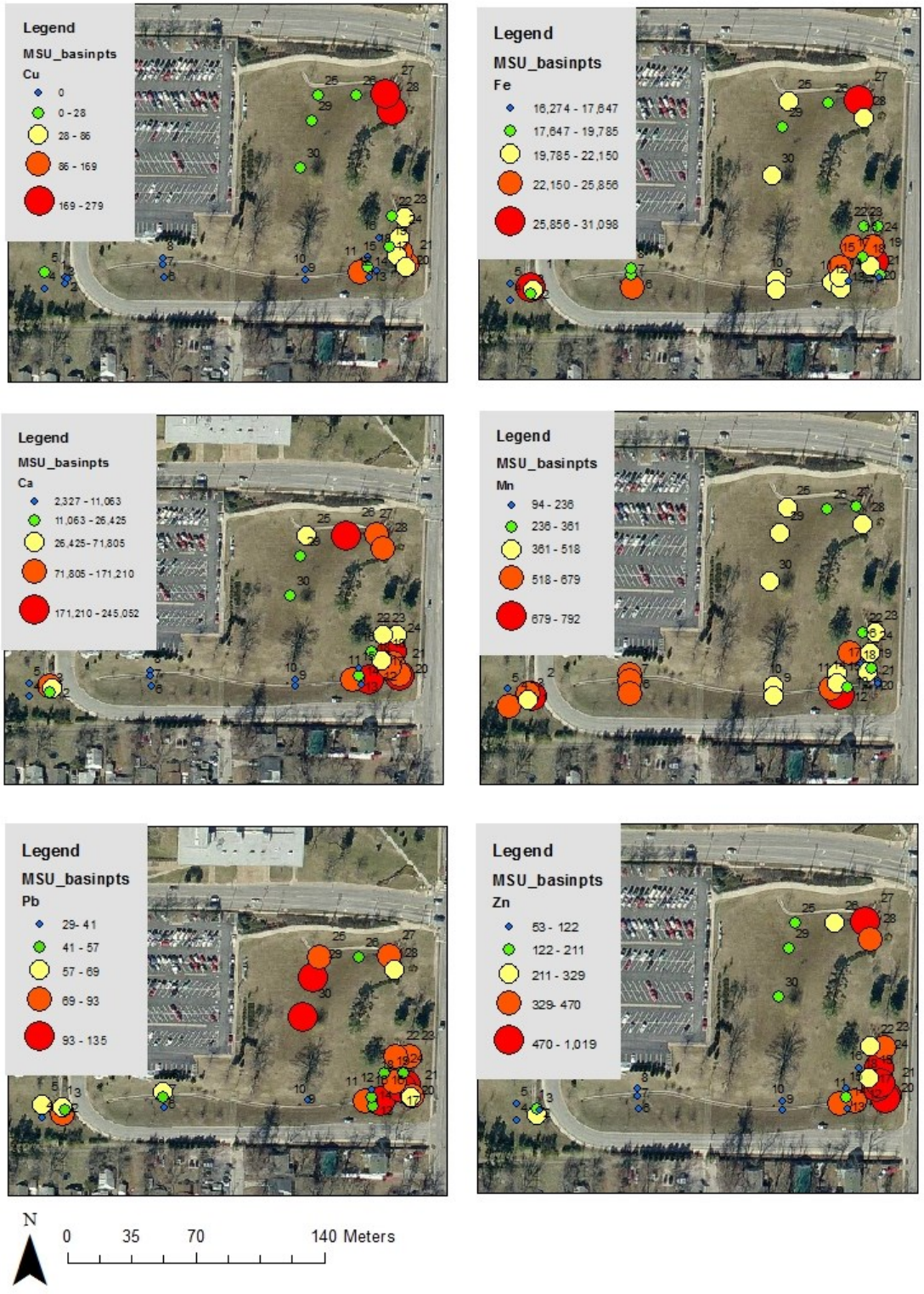

Fig. 21. Metal concentration distribution throughout the detention basin

Ring Number Analysis. The molecular structure was noted for each of the individual EPA_{16} molecules. To represent the weight and structure of the PAH molecule, the number of benzene rings found within the organic compound were listed. Ring counts for selected EPA_{16} samples were found to vary from 2-6 rings (Table 8). Concentrations for the individual EPA_{16} were calculated using PDC Laboratories raw data (Appendices A- 4-5). Individual PAHs with the highest average PAH concentrations were found to be the same for both 2015 and 2016 samples (Figures 22a-22b). The lowest individual PAHs were also found to be the same between the 2015 and 2016 samples based on average percent contribution. The lower molecular weights contributed significantly lower values to the total concentration found throughout the basin (Tables 9-10). This suggests that the individual EPA_{16} samples with fewer benzene rings, resulting in a lower molecular weight, were more likely to be transported away from the source (Mahler, et al., 2014). The average coal-tar and asphalt sealant percent distribution of the select PAHs from two previous studies is included in Tables 9-10 (Pavlowsky, 2012; Mahler et al., 2014).

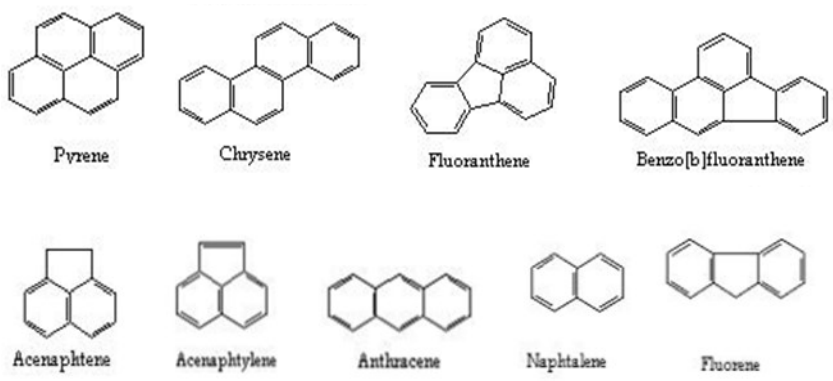

Fig. 22. The highest (top) and lowest (bottom) individual PAHs found within the samples (www.theadvocateproject.eu).

Table 8. Ring count for individual EPA_{16}

Rings	Individual PAHs
2	Acenaphthene
2	Acenaphthylene
2	Naphthalene
2(3)	Fluorene
3	Anthracene
3	Phenanthrene
3(4)	Fluoranthene
4	Benzo(a)anthracene
4	Pyrene
4	Chrysene
4(5)	Benzo(b)fluoranthene
4(5)	Benzo(k)fluoranthene
5	Benzo(g,h,i)perylene
5	Dibenzo(a,h)anthracene
5	Benzo(a)pyrene
5(6)	Indeno(1,2,3-cd)pyrene

Table 9. Highest individual PAHs found and percent contribution for each sampling set (Pavlowsky, 2012; Mahler et al., 2014)

Highest Individual PAHs	2015 (%)	2016 (%)	Coal-Tar (%)	Asphalt (%)
Pyrene	12.07	11.50	15.37	13.35
Fluoranthene	12.13	13.34	21.77	19.45
Chrysene	9.32	8.65	9.32	8.79
Benzo(b)fluoranthene	9.73	12.48	11.38	10.74

Table 10. Lowest individual PAHs found and percent contribution for each sampling set

Lowest Individual PAHs	2015 (%)	2016 (%)	Coal-Tar (%)	Asphalt (%)
Naphthalene	2.76	2.89	0.32	1.5
Acenaphthylene	2.76	2.89	0.03	0.05
Acenaphthene	2.76	2.89	0.94	1.5
Fluorene	2.76	2.89	1.26	1.85
Anthracene	2.76	2.89	3.17	2.57
Dibenzo(a,h)anthracene	3.36	3.10	0.61	0.69

Correlation Matrix. The first 30 sediment samples were correlated to observe the detailed relationships throughout the data. PAH concentrations, organic matter, and grain size were compared throughout these correlations. Pearson's R values were used as basis of comparison.

PAH concentrations showed a similar correlation with all three grain sizes (Table 11A). PAHs were negatively correlated with clay (-0.634) and silt (-0.68), but positively correlated with sand (0.689). Areas of highest sand percentages appeared to be located near the inlets and outlet regions, which is predominantly where increased PAH concentrations were found (Figures 16 and 19). This suggests that regions of high sand content are likely regions of increased PAH concentration.

Lead, Zn, Cu, and Ca showed significant correlations (Table 11A). The regions predominantly influenced by Pb, Zn, Cu, and Ca were in the SE outlet and at the Central inlet (Figure 21). Runoff sources which primarily contribute to these regions are road

runoff from Grand Street and National Avenue as well as the coal-tar sealed parking lot (Figure 6).

OM-LOI showed no significant correlation with any other variable, suggesting that organic matter has no apparent correlation with substrate type (Table 11A). Neither the organic matter nor heavy metals displayed strong correlation with PAH concentration for the total basin sample analysis (Table 11A). While it is expected that PAHs may correlate with organic matter (Syroventik et al., 2007; Yang et al., 2008; Srogi, 2007) data suggests that PAH concentration is not significantly influenced by the organic matter or metal types (Table 11A). However, channel and basin samples from the 2015 sampling were separated. Sand and PAH concentration had a positive correlation in channel samples, but showed no correlation in the basin samples (Table 11B and 11C). Organic matter showed to have a larger influence in basin sediment, insinuating that organic matter may influence the contaminant behavior (Table 11B).

Sources. PAH and metal concentrations were predominantly found in close relation to the inlet or outlet locations. PAHs showed a positive correlation with sand in all basins except the South sub-basin (Figure 16). This suggests that sand-sized particles may be indicative of regions with PAH contamination. This may be due to source contamination or the collection of sand-sized PAH particulates that had been abraded from the parking lot and deposited near the inlet (Figure 1).

Highest PAH concentrations were found in the West inlet and Central outlet (Figure 19). The SW inlet receives direct runoff from the coal-tar sealed lot (Figure 6). This runoff is transported directly to the SE outlet. The South sub-basin had low PAH values as well as low correlations (Table 4).

Table 11 A. Pearson R correlation of 2015 samples (n=30)

Sample Analysis	PAH	LOI	Pb	Zn	Cu	Fe	Mn	Ca	Sand	Silt	Clay
PAH	1	-0.13	-.020	-.195	-.214	.067	.153	-.178	.689**	-.680**	-.634**
LOI		1	-.022	.232	.267	-.022	-.336	.300	-.240	.255	.164
Pb			1	.479**	.256	-.037	-.335	.416*	-.021	-.015	.126
Zn				1	.774**	.287	-.551**	.779**	-.267	.228	.352
Cu					1	.304	-.326	.578**	-.285	.272	.287
Fe						1	.191	.195	.215	-.216	-.186
Mn							1	-.511**	.328	-.317	-.322
Ca								1	-.217	.202	.235
Sand									1	-.990**	-.909**
Silt										1	.843**
Clay											1

** Correlation is significant at the 0.01 level (2-tailed).

* Correlation is significant at the 0.05 level (2-tailed).

Table 11 B. Pearson R correlation of 2015 Basin samples (n=20)

Basin	PAH	LOI	Pb	Zn	Cu	Fe	Mn	Ca	Sand	Silt	Clay
PAH	1	0.467	0.118	0.146	0.161	0.235	-0.072	-0.042	0.167	-0.06	-0.324
LOI		1	0.201	0.514	0.627	0.41	-0.338	0.244	-0.186	0.206	0.053
Pb			1	0.568	0.275	0.03	-0.363	0.588	-0.124	0.025	0.28
Zn				1	0.762	0.341	-0.536	0.816	-0.079	-0.032	0.285
Cu					1	0.408	-0.258	0.627	-0.033	0.006	0.077
Fe						1	0.131	0.137	0.278	-0.271	-0.162
Mn							1	-0.548	0.199	-0.154	-0.201
Ca								1	-0.123	0.061	0.2
Sand									1	-0.94	-0.655
Silt										1	0.357
Clay											1

Table 11 C. Pearson R correlation of 2015 Channel samples (n=10)

Channel	PAH	LOI	Pb	Zn	Cu	Fe	Mn	Ca	Sand	Silt	Clay
PAH	1	-0.295	-0.037	-0.163	-0.212	-0.089	-0.094	-0.326	0.336	-0.348	-0.29
LOI		1	-0.318	0.138	0.202	-0.367	-0.465	0.452	-0.797	0.805	0.76
Pb			1	-0.033	0.054	-0.317	-0.312	-0.295	0.465	-0.457	-0.49
Zn				1	0.982	0.272	-0.518	0.717	-0.252	0.262	0.20
Cu					1	0.118	-0.554	0.642	-0.272	0.282	0.22
Fe						1	0.256	0.38	0.2	-0.198	-0.20
Mn							1	-0.437	0.132	-0.146	-0.07
Ca								1	-0.624	0.633	0.58
Sand									1	-1	-0.99
Silt										1	0.99
Clay											1

This sub-basin is the primary flow path for runoff water, which suggests that the PAH and contaminated particles within the South sub-basin are being flushed into the SE outlet (Figure 6). The SE outlet receives runoff from the road as well as runoff from the central basin and trickle channels. Road runoff may contain vehicular-transported or weathered coal-tar particles as well as incomplete combustion materials (Readman et al., 2002; Crane, 2013). These contaminants may enter into the basin through the stormwater drains or inlets and accumulate within the basin sediment (Srogi, 2007). The areas of highest PAH contamination are likely a result of coal-tar sealant contribution, but may also be influenced by additional sources such as incomplete combustion of fuels, windblown PAH particulates, or vehicular emissions (Ahrens and Depree, 2010; Readman et al., 2002; Mahler et al., 2005).

Metals similarly collected in the inlets or outlets (Figure 21). Copper, Ca, Pb, and Zn were all found in higher concentrations in the Central inlet and SE outlet. The Central inlet receives primary runoff from Grand Street and National Avenue. The SE outlet receives its sources from the entirety of the basin, including the northern inlet. Metals commonly contributed from cars are Pb, Zn, Fe, Cu, Cd, Cr, Ni, and Al (Conservation Currents, Northern Virginia Soil and Water Conservation District, 2017). This suggests that these metals may primarily be contributed from the roads compared to the coal-tar lot. Calcium, however is commonly added to the environment through construction (Martin et al., 2015). Limestone is often added to cement mixtures as a binding agent (Martin et al., 2015). Recent and ongoing construction across the MSU campus has likely contributed loose particulates of this disrupted cement into the basin through runoff, increasing the Ca concentration throughout the basin.

Alternatively, Mn and Fe had higher concentrations near West inlet, Central outlet, and South sub-basins (Figure 21). PAHs have been found to bind to the Fe and Mn- oxide coatings on substrate such as sand and silt (Tessier et al., 1979). This suggests that a possible relationship between the locations of Fe and Mn relates to the binding of Fe and Mn-oxides with PAHs (Tessier et al., 1979). Also seen in Figure 21, Pb shows significant concentrations in the central basin ranging from 69 – 135 ppm. As seen in aerial photos (Figure 7), the basin was comprised of houses and parking lots. Lead additives in gasoline were not officially prohibited until 1996, suggesting that a contributor of the lead in the central basin may be from previously leaded gasoline (Newell and Rogers, 2003). Lead-based paint was used in homes and buildings until 1978, when it was banned for being a health hazard (Centers for Disease Control and Prevention, 2014; Agency for Toxic Substances and Disease Registry, 2007). Houses in the basin likely contributed lead into basin soil, due to the age at which they were built.

The pH values collected were found to range between a pH value of 7.1 - 7.5 (Table 12). Soil is considered to be strongly acidic and harmful to plant growth when it reaches a pH value between 4.0-5.0 (Bickelhaupt, 2017). Determined pH values suggested that acidity levels of basin soils ranged from neutral to weakly alkaline (Bickelhaupt, 2017). The primarily neutral pH values suggest that the acidity of the basin soil has no significant influence on the contaminants in the basin (Faure, 1998; Silberg, 2010). Due to this, it can be assumed that the acidity levels of the basin soil and sediment are insignificant in relation to the results.

Table 12. pH values determined for select samples and substrate

Core	Sample	pH	RPD (%)	Sediment Type
1	31	7.3		Silt
1	33	7.2		Mud
1	35	7.1		Clay
2	37	7.5		Mud/silt
2	38(1)	7.1	-1.4	Clay
2	38(2)	7.2		Clay
2	39	7.4		Clay
2	41	7.4		Clay/mud
3	42	7.2		Mud
3	44	7.5		Mud/silt
3	46(1)	7.1	-1.4	Mud
3	46(2)	7.2		Mud
DI Blank	DI Blank	7.3		DI Blank
3	48	7.3		Clay & mud

Core Analysis

Three sediment cores were collected throughout the sediment basin as well as a duplicate core near each PAH-analyzed core (Figure 23, C). Core one was taken in the Central outlet region, core two (A) was collected in the SE corner of the basin near the trickle channel, and core three was taken in the West inlet sub-basin near the coal-tar inlet near the trickle channel (B).

A

B

C

Fig. 23. Core 2 location (A) core 3 location (B) and example of sediment core sampled (C)

PAH Core Values. No values were below the non-toxic range of 1,610 µg/kg, but 67% of the samples were found to be above the toxic threshold of 22,800 µg/kg (Table 13; Appendix A-2) (Macdonald et al., 2000). Roadside samples had the highest maximum concentration yielding 534,650 µg/kg followed by Core 2 with a maximum value of 220,600 µg/kg in the upper most 5 cm of the core sediment (Table 4; Figures

24a-24c). Core 3 was found to have the lowest determined value with a minimum value of 3,200 µg/kg (Table 4). The value of 3,200 µg/kg was found in the 25-35 cm range in depth (Figures 24a-24c).

PAH concentrations showed a continuous decrease with the increase in depth, diminishing at the depth of 27-35 cm whereas the regions of highest contamination were found within the upper 0-10 cm (Figures 24a-24c). This shows that the depth of contamination is relatively shallow throughout the basin.

Table 13. PAH_{16} concentration of core samples

Core	Depth (cm)	PAH Concentration (µg/kg)
1	0-10	79,450
1	10-15	54,450
1	15-20	72,700
1	20-25	61,150
1	25-30	12,950
2	0-10	220,600
2	10-15	136,200
2	15-20	48,250
2	20-25	29,290
2	25-30	37,330
2	30-35	21,670
3	0-10	206,300
3	10-15	119,400
3	15-20	51,400
3	20-25	9,250
3	25-30	3,200
3	30-35	3,200
3	35-40	3,200

2016 Sediment Core Metal Values. The metal concentrations for core samples were calculated using same methods (Appendices B-2 and B-3). The maximum concentrations of Pb and Zn values were found in the roadside samples, with a maximum Pb concentration of 349 ppm and a Zn concentration of 643 ppm (Table 14). The lowest Pb and Zn values were located in Core 3, with a Pb concentration of 83 ppm and a Zn value of 147 ppm (Table 14). The highest Cu concentration was located in Core 2, with a concentration of 68 ppm (Table 14) followed closely by a concentration of 63 ppm in the roadside samples (Table 14). The lowest Cu concentration was located in Core 3, which stated that there were no detectable Cu values (< DL) (Table 14). Iron values appeared to be very high throughout all samples, but the highest recorded value was located in Core 2, with a concentration of 33,929 ppm (Table 14). The lowest Fe value was found to be 20,453 ppm, in Core 3 (Table 14). Core 1 had the highest Mn value with a concentration of 1,087 ppm (Table 14). Core 3 showed the lowest concentration of Mn, with a maximum value of 872 ppm (Table 14). The highest Ca values were located in the roadside samples, with a mean concentration of 283,687 ppm (Table 14). The lowest Ca values were found to be in Core 3, with a maximum concentration of 41,843 ppm (Table 14). The response of metal concentrations with the increase was analyzed for both the PAH-analyzed core and duplicate core (Tables 15-16).

Table 14. Metal values for core and road samples

Sample Location		n	Pb (ppm)	Zn (ppm)	Cu (ppm)	Fe (ppm)	Mn (ppm)	Ca (ppm)
Core 1		5						
	Maximum		111	541	53	30,154	1,087	73,460
	Median		71	346	34	20,792	798	52,945
	Minimum		43	65	20	18,889	583	4,547
Core 2		6						
	Maximum		115	541	68	33,929	1,049	110,488
	Median		92	242	33	25,579	652	37,209
	Minimum		62	110	16	19,367	136	16,316
Core 3		7						
	Maximum		83	145	< DL	20,453	872	41,843
	Median		64	111	< DL	19,487	536	14,415
	Minimum		37	21	< DL	15,646	451	2,592
Roads		6						
	Maximum		349	643	63	30,126	1,003	283,687
	Median		114	572	31	23,806	381	77,459
	Minimum		35	98	28	15,019	242	6,038

Table 15. Metal concentration in response to depth

Core	Depth (cm)	Pb (ppm)	Zn (ppm)	Cu (ppm)	Fe (ppm)	Mn (ppm)	Ca (ppm)
1	0-10	71	429	37	20,792	660	60,132
	10-15	111	541	53	30,154	1,087	73,460
	15-20	73	346	31	20,837	798	52,945
	20-25	61	198	20	19,316	894	29,477
	25-30	43	65	< DL	18,889	583	4,547
2	0-10	104	541	67	19,367	631	110,488
	10-15	70	180	16	25,198	1,049	34,350
	15-20	62	110	< DL	33,929	715	16,316
	20-25	115	234	17	31,416	336	32,700
	25-30	83	250	33	25,959	136	40,067
3	0-10	65	141	< DL	19,487	536	37,085
	10-15	76	145	< DL	20,103	644	41,843
	15-20	62	115	< DL	18,626	518	28,288
	20-25	83	111	< DL	20,020	534	14,415
	25-30	37	51	< DL	16,174	872	4,574
	30-35	< DL	21	< DL	15,646	451	2,592

Table 16. Duplicate core metal concentration in response to depth

Duplicate Core	Depth (cm)	Pb (ppm)	Zn (ppm)	Cu (ppm)	Fe (ppm)	Mn (ppm)	Ca (ppm)
1	0-10	66	356	43	21,696	909	44,923
	10-15	103	360	33	20,800	845	58,471
	15-20	60	144	13	21,823	854	18,291
	20-25	44	104	10	22,427	866	17,709
	25-30	40	113	15	22,302	630	23,103
2	0-10	113	510	72	19,371	531	111,592
	10-15	94	363	52	20,529	576	72,262
	15-20	76	199	20	23,081	844	37,307
	20-25	69	138	< DL	29,188	929	23,673
3	0-10	58	143	< DL	18,307	531	32,586
	10-15	62	120	< DL	19,953	551	31,835
	15-20	89	113	< DL	20,444	749	16,898
	20-25	93	129	< DL	24,338	854	13,337
	25-30	111	105	< DL	22,413	957	9,011
	30-35	112	129	< DL	21,514	732	10,152

2016 OM-LOI Core Values. The highest regions of OM-LOI were found to be in Core 2 (Appendix D-2), reaching 12.9%, and road-side samples with a maximum of 14.9%. Core 3 had the lowest percentage of OM-LOI with a maximum of 8%. Agreeing with the maximum and minimum values, average values of the cores showed matching results for highest and lowest OM-LOI values of the sediment cores taken. Duplicate core values (Appendix D-3), which did not include road-side samples, supported the previous findings indicating the region with highest OM-LOI for the core samples is Core 2 in the Central inlet and Core 3 has the lowest value is in the West inlet.

Cesium – 137 (Cs-137). Cesium activity values for core one ranged from a minimum of 8.4 to a maximum of 13.5 Bq/kg (OEWRI SOP). Core two activity ranged from a minimum of 6.6 Bq/kg to a maximum of 10.7 Bq/kg (Table 17). Core three had an

activity range of 5.0 Bq/kg to 9.1 Bq/kg (Table 17). Cs-137 values showed no distinct patterns with depth (Figures 24a-24c). Due to the weaker activity values and no significant trends with the increase in depth, this suggests that this is a young basin which has been disturbed. The disturbances have homogenized the basin soil, disrupting the expected trend of Cs-137 dating back to approximately 1963 (USGS, 2016).

Table 17. Sediment core Cs-137 activity and uncertainty values

Sample	Core	Depth (cm)	Mass (kg)	Activity (Bq/kg)	Uncertainty (Bq/kg)	Activity RPD (%)	Uncertainty RPD (%)
31(1)	1	3	0.2	12.0	0.5		
31(2)	1	3	0.2	11.2	0.5	1.8	0.8
32	1	7	0.1	8.4	1.0		
33	1	15	0.2	11.8	0.5		
34	1	20	0.1	12.7	0.6		
35	1	25	0.1	13.5	0.8		
36	2	5	0.1	7.8	1.4		
37	2	10	0.1	10.7	1.3		
38A	2	15	0.1	6.6	0.9		
42	3	5	0.1	7.9	0.6		
43	3	10	0.1	7.4	0.5		
44(1)	3	15	0.1	5.0	0.9		
44(2)	3	15	0.1	7.3	0.5	-9.4	11.4
45	3	20	0.1	5.5	0.6		
46	3	20	0.1	6.2	0.8		
47	3	28	0.1	9.1	0.5		

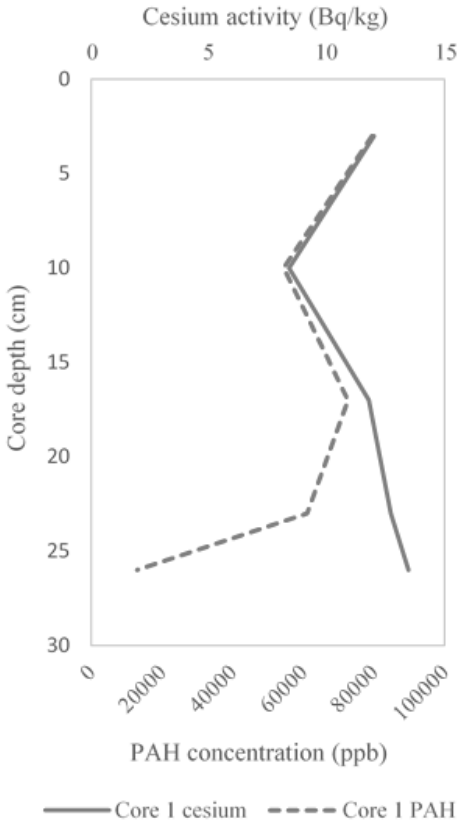

Fig. 24a. PAH concentration and Cs-137 activity with depth for core

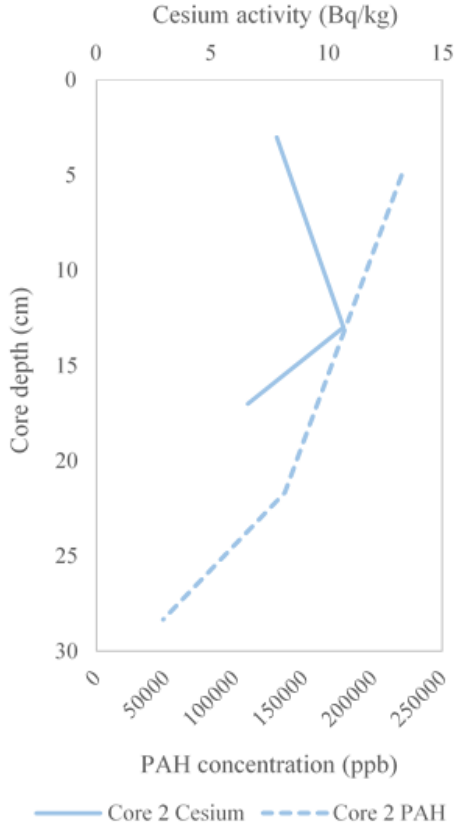

Fig. 24b. PAH concentration and Cs-137 activity with depth for core

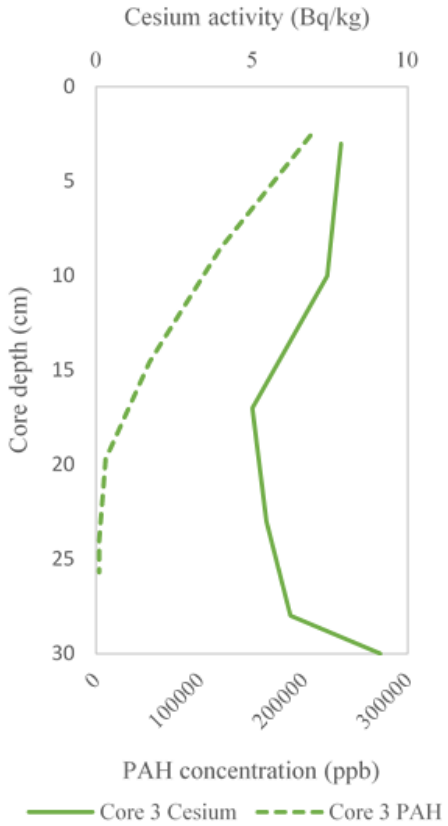

Fig. 24c. PAH concentration and Cs-137 activity with depth for core 3

Management Implications

Urban stormwater basins can trap fine-grained sediment and associated pollutants (Guo, 1997; Birch et al., 2006). However, trap efficiency may vary from basin to basin depending on the design and residence time of water in the basin to allow for settling of suspended particles to take place (Birch et al., 2006). Basins that accumulate sediment can reduce pollution risk to downstream waters, while those that pass contaminants freely offer little protection to receiving water bodies (Fischer et al., 2003). To evaluate the effect of the present basin to reduce off-site pollutant transport, estimated annual loadings of PAHs to the basin were compared to the mass of PAHs stored in basin soils and channel deposits. If stored rates are relatively high, then some level of pollution control is assumed.

To understand the amount of PAHs contributed by coal-tar sealants within a 3-5 year time period, the mass of coal-tar sealant needed to cover an area (kg) and the amount of PAHs within that area (mg/kg) were calculated. Coal-tar sealant has a bulk density of 1.15 g/cm^3. Approximately 0.89 l/m^2 of coal-tar sealant is applied on a parking lot on average (Yang et al., 2010; EPA, 2012; Star-Seal of Florida inc., 2014). Coal-tar sealcoat typically contains at least 20% coal-tar pitch, which is 50% or more PAHs by mass (EPA, 2012). Further, up to 50% of PAHs may volatilize from curing sealcoat within 1-2 months after application (Van Metre et al., 2012). Using these assumptions, 52.2 grams/m^2 PAHs are applied to parking lots on average. Therefore, the 0.048 km^2 of coal-tar sealed parking lots in the catchment contribute 2,487 kg of PAHs throughout a 4-year time period (Table 18). This results in approximately 621 kg/yr of PAHs annually contributed by the coal-tar sealed parking lots within the sub-watershed. PAH

contributions from coal-tar lots are 100 to 1000 times higher than PAH contributions from concrete or asphalt lots (USGS, 2011; Mahler et al., 2014). Therefore, annual PAH loads from coal-tar lots reflect > 95% of the total PAH load to the basin.

Table 18. Parking Lots in watershed contribution of PAHs into watershed

Parking Lot	Sub-Watershed	Area (m^2)	PAHs (g)	PAHs (kg)
1	North	1,408	73,542	73
16	North	754	39,369	40
14	North	6,507	339,702	340
9	North	1,849	96,518	97
29	North	9,131	476,665	477
22 & 24	West	28,000	1,461,600	1461
Total		47,649	2,487,396	2,487

The mass storage of sediment was calculated for basin soil and trickle channels by multiplying the volume of the sub-basin by the soil bulk density. A bulk density of 1.4 g/cm^3 was used for soils and sediment in this study since soils in this area have bulk density values from 1.3-1.5 g/cm^3 (Hughes, 1982). Seen in Figure 25, sediment depths of the West, South, Central Outlet, and Central sub-basins (n=10) were measured with a tile probe (Table 18). Trickle channels were accounted for separately, which resulted in West inlet, South, Central outlet, and the North trickle channel (n=4). The dredged sediment (5 m^3) in the spring of 2016 was incorporated into calculations, using the median values of the PAH concentrations within the basin Central outlet sub-basin (Table 19).

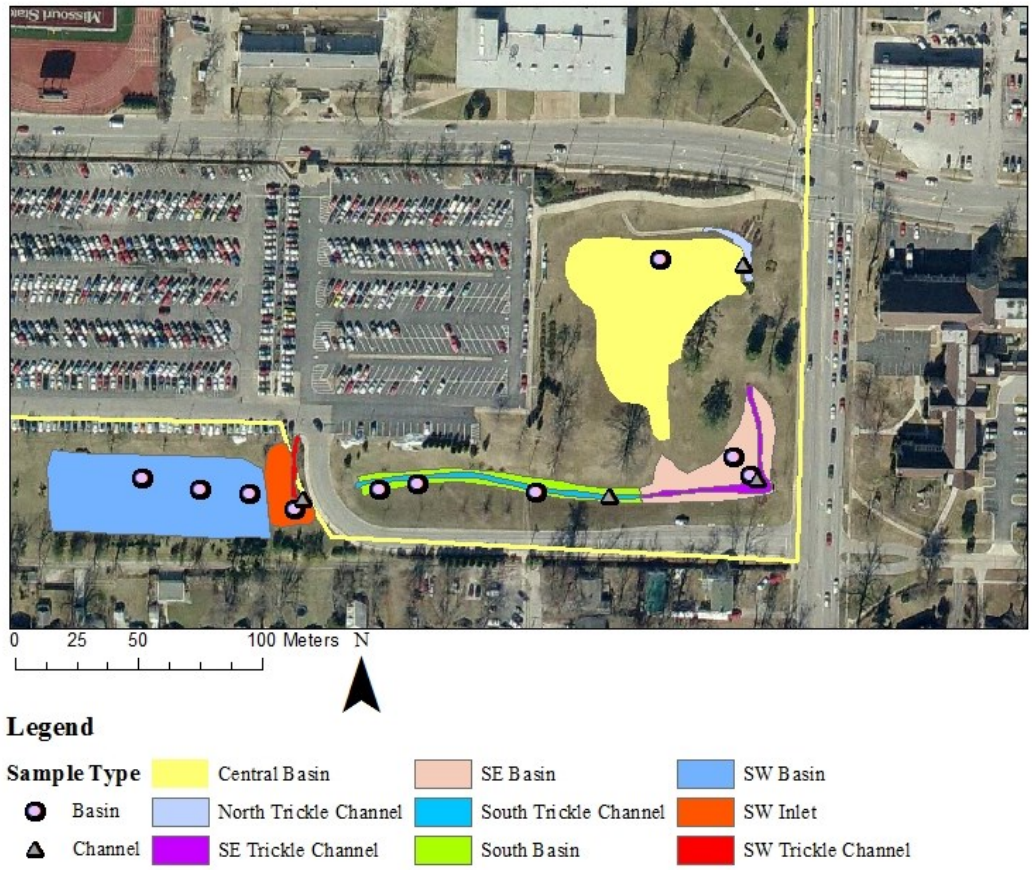

Fig. 25. 2017 probe depths taken throughout basin floor and trickle channel regions

Because all 2015 surface samples were collected to a maximum depth of 5 cm, a depth of 5 cm was assigned to the basin samples for the PAH mass storage calculation (Table 19). PAH mass storage was calculated by multiplying the median PAH concentration of each sub-basin by its respective mass sediment storage. Probe depths were used to identify recent sediment deposits throughout the basin soil area (not used for mass storage calculation) ranged from 1 – 4 cm in depth. This indicates sedimentation ranges from 0.6 - 2.4 mm/year, based on the 17 year accumulation of the basin. Trickle channel sediment storage was calculated using the probe depths collected in the spring of 2017 (Figure 25). Results showed that a total of 21 kg of PAHs were stored within the

basin with an annual storage rate of 1.2 kg/yr (Table 19 and Table 20). It can be assumed that the basin has retained < 1% of the coal-tar introduced by runoff. This suggests that the 99% of the PAHs are transported out of the basin outlet to contaminate local streams. However, this calculation is based on the assumption that all of the sealant on the parking lots was removed and delivered to the basin by runoff after volatilization losses were considered.

Table 19. Basin soil storage of PAHs (kg)

Sub-Basin	Depth (cm)	Area (m^2)	Volume (m^3)	Sediment Mass Storage (kg)	n	PAHs Avg. (ug/kg)	PAH mass (kg)
West Inlet	5	404	20	30,271	-	-	-
West	5	2,848	142	213,614	3	39,497	8
South	5	507	25	38,037	5	11,300	0
Central Outlet	5	990	50	74,263	8	39,676	3
Central	5	3,205	160	240,411	4	24,810	6
Dredged (July 26, 2016)	5	990	5	7,000	8	39,676	0
Total		7,955	402	603,596			17

Table 20. Channel sediment storage of PAHs (kg)

Trickle Channel	Probe Depth (cm)	Area (m^2)	Volume (m^3)	Sediment Mass Storage (kg)	n	PAHs(ug/kg)	PAH mass (kg)
West Inlet	1	71	0.02	3,175	2	397,700	1
South	2	217	0.01	3,249	-	-	-
Central Outlet	2	203	0.25	9,153	6	275,983	3
Central	1	102	0.08	7,664	2	145,300	1
Total		593	0.36	23,241			4

CONCLUSIONS

PAH contamination in rural and urban regions has been extensively studied, as well as the correlation to coal-tar sealants (Crane, 2013; Boffetta et al., 1997; Eisler, 1987; Krein and Schorer, 2000; Mahler et al., 2014). Coal-tar sealants are one of the leading contributors of PAHs into the environment, and have been found to contaminate sediment with PAH concentrations approximately 1,000 times higher than asphalt-based sealants (Eisler, 1987; USGS, 2011; McKinney, 2012; Crane, 2013; Van Metre and Mahler, 2013; EPA, 2016). Despite the environmental concerns, coal-tar sealants are still commonly used throughout society (Crane, 2013).

Missouri State University has used coal-tar sealants throughout the campus region over the past 20 years. However, there has not been a reapplication in the last 1.5 years (Missouri State University Campus Facilities, 2016). This study evaluated the PAH contaminated trends in an urban stormwater basin on campus that drains 0.22 km^2 with coal-tar sealed parking lots contributing 22% of the drainage. Contaminants such as PAHs and heavy metals have been accumulating within this specific basin for approximately 17 years. Sediment PAH concentrations exceed toxic limits in most cases. While PAHs are stored in sediment deposits and soils in the basin, most PAHs delivered to the basin by stormwater pass through it and into local streams.

The main findings of this study include:

1. There is significant sediment-PAH contamination throughout the basin. PAH concentrations in basin soils and sediments ranged from 3,200- 712,500 µg/kg (Appendix A-1). Sixty-five percent of samples exceeded the PAH toxicity limit for sediment-dwelling organisms of 22,800 µg/kg (MacDonald et al., 2000). No samples were found to be below the non-toxic limit of 1,610 µg/kg, suggesting

that all samples collected and analyzed pose a threat to the surrounding environment (Crane, 2013; Eisler, 1987; MacDonald et al., 2000).

2. Highest PAH concentrations occurred in sediment deposits in the trickle channel and aggraded deposits near sub-basin inlets and outlets. PAH concentrations were lower in basin soils compared to channel deposits and in Central sub-basin (11% of drainage area from a coal-tar lot) compared to West sub-basin (70% of drainage area from a coal-tar lot). This suggests that PAH-contaminated sediment is transported throughout the basin and that it is primarily contributed from coal-tar sealed lots.

3. The highest concentrations were found for high molecular weight PAHs (4-6 rings) with each contributing 9-13% of the total PAH_{16} concentrations. Low molecular weight PAHs (2-3 rings) only contributed about 3% each. This agrees with previous studies which have shown that lower molecular weight PAHs contribute a smaller amount of total accumulated PAHs due to their higher transport and volatility capability (Mahler et al., 2014). However, the difference in concentration of individual EPA_{16} may also be due to source supply. The coal-tar sealant may contribute larger quantities of high molecular weight PAHs compared to the low molecular weight PAHs.

4. Grainsize analysis indicated correlation between sand-sized particles and PAH concentration within channel samples. Sand and PAH particulates are deposited in the trickle channels by flood events. Alternatively silt and clay, specifically clay, were primarily found throughout the basin soil and generally showed weaker correlations with PAHs. Sand is predominantly found within the channel systems, as well as the highest PAH concentrations (Figure 16 and 19). Sand-sized particles are likely weathering products released from degrading roadways and other urban surfaces. However, PAH-containing particles tend to be preferentially deposited in the trickle channels, along with sand grains (EPA, 2016; Mahler et al., 2005; Pavlowsky, 2013). Therefore, both sand and sediment particles tend to be deposited together in the trickle channels of the basin. The process by which this happens is unclear and needs to be studied further.

5. Metal concentrations were influenced by three main sources: urban runoff, groundwater seepage, and eroded sediment supplied from natural or construction materials. Metal concentrations were determined for Zn (53-1,019 ppm), Cu (<DL- 279 ppm), Fe (16,274-31,098 ppm), Mn (94-792 ppm), Pb (29-135 ppm) and Ca (2,327-245,052 ppm). Copper, Zn, Fe, and Pb are commonly contributed by cars exhaust and wear, suggesting that vehicles and urban surface weathering may be a significant source of these metals entering the basin (Conservation Currents, Northern Virginia Soil and Water Conservation District, 2017). Iron and Mn were found in higher concentrations near a naturally occurring spring in the West sub-basin. This suggests that they may be contributed naturally from the local groundwater seepage. Elevated calcium concentrations were likely caused by the addition of eroded particles from concrete and other pavement surfaces.

6. Organic matter-PAH relationships are stronger in basin soil area and weaker in channel sediment. Channel sediment samples showed an R value of -0.29 correlation between PAH and LOI. Alternatively, PAH and LOI correlations in basin soil samples was 0.47 (Table 11B and 11C). Basin soil samples showed a median value range from 10.1 to 11.5% compared to channel sediment, which ranged from 5.6 to 11.2%. Organic matter relationships follow similar patterns from previous studies (Syroventik et al., 2007; Srogi, 2007). Further studies are needed to observe definite trends.

7. Core samples collected from locations of relatively high sediment deposition were typically contaminated with PAHs to depths of 0.25-0.35 m with concentrations decreasing with depth. However, the depth of PAH contamination in the basin is typically < 5 cm. Additionally, the basin soils contained weak Cs-137 activity with no obvious trends indicating recent age as expected (Figure 24a -24c). Coal-tar sealants were found to be one of the leading causes for PAH contamination throughout urban watersheds beginning in the 1960s (USGS, 2011; USGS, 2015). Assuming that additional sources of PAHs have remained consistent, the intensified popularity and use of coal-tar sealants since the 1960s is a likely cause for the increase in PAH concentrations in basin cores (USGS, 2015).

8. Only < 1% of the PAH mass from urban runoff including coal-tar lots is being stored in the detention basin annually. These findings suggest that while the majority of the PAHs are contributed by coal-tar sealed parking lots, they are not being deposited or stored for long-term periods in the basin, but are transported downstream into Fassnight and Wilson Creeks to possibly contribute to water quality problems.

This study found that there are toxic levels of PAHs and elevated concentrations of metals within the detention basin. This supports previous studies which stated that detention basins often retain increased concentrations of contaminants (Guo, 1997; Birch et al., 2006). Significant amounts of PAHs are contributed by runoff from coal-tar sealed parking lots. Highest concentrations of PAHs were found in the West sub-basin where coal-tar sealed lots cover approximately 70% of the drainage area and roads only 7% (Figure 11). Lower PAH concentrations are found in the Central sub-basin area with 11% lot cover and higher road coverage including direct drainage from high traffic Grand Street and National Avenue. Therefore, coal-tar lots represent major sources of PAHs to

this basin. These results may be generally extrapolated to other urban stormwater detention basins, but more studies are needed. Specific sources of PAHs to the basin were not directly evaluated in this study.

Future Work

This study provided a detailed analysis of basin sediment contamination and sediment-PAH relationships. However, this study did not quantify dissolved or particulate PAHs in runoff. Future research may include the collection of stormwater runoff from the various inlets to observe how the PAH concentrations are dispersed from the inlets throughout the basin (McCarthy and Zachara, 1989; Walsh et al., 2005). Understanding the rate at which accumulation is occurring may result in the exploration of bioremediation techniques possible for this basin (Piskonen and Itavaara, 2004; Haritash and Kaushik, 2009). Additional sample collection and analysis may verify the trends reported by this study or provide new insights into PAH distribution patterns and processes.

REFERENCES

Abdel-Shafy, H. I. and Mansour, M. S. M., 2016, A review on polycyclic aromatic hydrocarbons: Source, environmental impact, effect on human health and remediation: Egyptian Journal of Petroleum, v. 25, p. 107-123.

Agency for Toxic Substances and Disease Registry, 2007, Lead Toxicity: https://www.atsdr.cdc.gov/csem/csem.asp?csem=7&po=5.

Ahrens, M. J., and Depree, C. V., 2010, A source mixing model to apportion PAHs from coal tar and asphalt binders in street pavements and urban aquatic sediments: Chemosphere, v. 81, p. 1526-1535.

Andronikov, S.V., Davidson, D.A., and Spiers, R.B., 2000. Variability in contamination by heavy metals: sampling implications. Water, Air, and Soil Pollution v. 120, p. 29-45.

Baumann, P. C., and Harshbarger, J. C., 1995, Decline in liver neoplasms in wild brown bullhead after coking plant closes and environmental PAHs plummet: Environmental Health Perspectives, v. 103.2, p. 168-170.

Birch, G. F., Matthai, C., and Fazeli, M. S., 2006, Efficiency of a retention/detention basin to remove contaminants from urban stormwater: Urban Water Journal, v. 3, issue 2, p. 69-77.

Bickelhaupt, D., 2017, Soil pH: What it means: http://www.esf.edu/pubprog/brochure/soilph/soilph.htm.

Bixian, M., Jiamo, F, Gan, Z., Zheng, L. Yushun, M., Guoying, S., and Xingmin, W., 2001, Polycyclic aromatic hydrocarbons in sediments from the Pearl river estuary, China: spatial and temporal distribution and sources: Applied Geochemistry, v. 16, p. 1429-1445.

Boffetta, P., Jourenkova, N., and Gustavsson, P., 1997, Cancer risk from occupational and environmental exposure to polycyclic aromatic hydrocarbons: Cancer Causes and Control, v. 8, p. 444-472.

Cardell, C., Benavente, D., and Rodriguez-Gordillo, J., 2008, Weathering of Limestone Building Material by Mixed Sulfate Solutions. Characterization of Stone Microstructure, Reaction Products and Decay Forms, Materials Characterization, v. 59, p. 1371-1385.

Centers For Disease Control and Prevention, 2014, Lead: https://www.cdc.gov/nceh/lead/tips.htm.

Choi, H., Harrison, R., Komulainen, H., and Delgado Saborit, J., 2010, Polycyclic aromatic hydrocarbons: WHO Guidelines for Indoor Air Quality: Selected Pollutants. Geneva: World Health Organization.

Comair, G. F., McKinney, D. C., and Siegel, D., 2012, Hydrology of the Jordan River Basin: Watershed delineation, precipitation and evapotranspiration: Water Resource Management, v. 26, p. 4281-4293.

Conservation Currents, Northern Virginia Soil and Water Conservation District, 2017.

Crane, J. L., 2013, Source apportionment and distribution of polycyclic aromatic hydrocarbons, risk considerations, and management implications for urban stormwater pond sediments in Minnesota, USA: Archives of Environmental Contamination and Toxicology, v. 65.4.

Di Stefano, C., Ferro, V., and Mirabile, S., 2010, Comparison between grain-size analyses using laser diffraction and sedimentation methods: Biosystems Engineering, v. 106, p. 205-215.

Easterbrook, D. J., 1999, Surface processes and landforms: Upper Saddle River, New Jersey, Prentice Hall, Inc., p. 27-29, 187-208.

Eisler, R., 1987, Polycyclic aromatic hydrocarbon hazards to fish, wildlife, and invertebrates: A synoptic review: U.S. Fish and Wildlife Service Biological Report 85(1.11).

EPA, 2012, Coal-tar sealcoat, polycyclic aromatic hydrocarbons, and stormwater pollution: Stormwater Best Management Practice: https://www3.epa.gov/npdes/pubs/coaltar.pdf.

EPA, 2016, Coal-tar sealcoat, polycyclic aromatic hydrocarbons, and stormwater pollution; Stormwater Best Management Practice: https://www.epa.gov/sites/production/files/2016-01/documents/sw_bmp_coal-tar_sealcoat-jan_16_508.pdf.

Faure, G., 1998, Principles and applications of geochemistry: Upper Saddle River, New Jersey, Prentice Hall, Inc., p. 118-124, 200-204.

Feng, J., Yang, Z., Niu, J., and Shen, Z., 2007, Remobilization of polycyclic aromatic hydrocarbons during the resuspension of the Yangtze River sediments using a particle entrainment simulator: Environmental Pollution, v. 149, issue 2, p. 193-200.

Fischer, D., Charles, E., and Baehr, A., 2003, Effects of stormwater infiltration on quality of groundwater beneath retention and detention basins: Journal of Environmental Engineering, v. 129, issue 5, p. 465-471.

Gan S., Lau, E. V., and Ng, H. K., 2009, Remediation of soils contaminated with polycyclic aromatic hydrocarbons (PAHs): Journal of Hazardous Materials, v.172, issue 2-3, p. 532-549.

Gaur, V. K., Gupta, S. K., Pandey, S. D., Gopal, K., and Misra, V., 2005, Distribution of heavy metals in sediment and water of River Gomti: Environ Monit Assess, v. 102, p. 419–433.

Gowd, S. S., Reddy, M. R., and Govil, P. K., 2010, Assessment of heavy metal contamination in soils at Jajmau (Kanpur) and Unnao industrial areas of the Ganga Plain, Uttar Pradesh, India: Journal of Hazardous Materials, v. 174, issue 1-3, p. 113-121.

Gu, S. H., Kralovec, A. C., Christensen, E. R., and Van Camp, R. P., 2003, Source apportionment of PAHs in dated sediments from the Black River, Ohio: Water Research, v. 37, p. 2149-2161.

Guo, Q., 1997, Sediment and heavy metal accumulation in dry detention basin: Journal of Water Resources Planning and Management, v. 123, issue 5, p. 295-301.

Han, G., and Liu, C., 2004, Water geochemistry controlled by carbonate dissolution: a study of the river waters draining karst-dominated terrain, Guizhou Province, China: Chemical Geology, v. 204, p. 1-21.

Haritash, A. K., and Kaushik, C. P., 2009, Biodegredation aspects of Polycyclic Aromatic Hydrocarbons (PAHs): A review: Journal of Hazardous Materials, v. 169, p. 1-15.

Hoffman, E. J., Mills, G. L., Latimer, J. S., and Quinn, J. G., 1984, Urban runoff as a source of polycyclic aromatic hydrocarbons to coastal waters: Environmental Science and Technology, v. 18, p. 580-587.

Howari, F. M., and Banat, K. M., 2000, Assessment of Fe, Zn, Cd, Hg, and Pb in the Jordan and Yarmouk river sediments in relation to their physicochemical properties and sequential extraction characterization: Water, Air, and Soil Pollution, v. 132, p. 43-59.

Howsam, M., and Jones, K. C., 1988, Sources of PAHs in the environment: PAHs and Related Compounds, Springer Berlin Heidelberg, p. 137-174.

Hughes, H. E., 1982, Soil survey of Greene and Lawrence Counties, Missouri: United States Department of Agriculture, p. 152-154.

Hwang, H., and Foster, G. D., 2006, characterization of polycyclic aromatic hydrocarbons in urban stormwater runoff flowing into the tidal Anacostia River, Washington, DC, USA: Environmental Pollution, v. 140, p. 416-426.

Irwin, R. J., VanMourweik, M., Stevens, L., et al., 1997, Environmental contaminants encyclopedia. National Park Service, Water Resources Division: https://nature.nps.gov/hazardssafety/toxic/pahs.pdf.

Jacobson, R. B., and Coleman, D. J., 1986, Stratigraphy and recent evolution of Maryland Piedmont flood plains: American Journal of Science, v. 286, p. 617-637.

Khadhar, S., Higashi, T., Hamdi, H., Matsuyama, S., and Charef, A., 2010, Distribution of 16- EPA-priority polycyclic aromatic hydrocarbons (PAHs) in sludges collected from nine Tunisian wastewater treatment plants: Journal of Hazardous Materials, v. 183, p. 98-102.

Kiner, L. K., and Vitello, C., 2016, James River; Watershed Inventory and Assessment: http://mdc.mo.gov/node/11121.

Kooistra L., Lueven, R.S.E.W., Nienhuis, P.H., Wehrens, R., and Buydens, L.M.C., 2001. A procedure for incorporation spatial variability in ecological risk assessment of Dutch River floodplains. Environmental Management, v. 28, p. 359-373.

Krein, A., and Schorer, M., 2000, Road Runoff pollution by polycyclic aromatic hydrocarbons and its contribution to river sediments: Water Research, v. 34, p. 4110-4115.

Lecce, S. A., and Pavlowsky, R. T., 2001, Use of mining-contaminated sediment tracers to investigate the timing and rates of historical floodplain sedimentation: Geomorphology, v. 38, p. 85-108.

Li, X. and Chen, X., 2007, Biodegradation of polysaccharide sourced from virulence factor or plant and pathogenic cell wall constituent and its application in management of phytopathogenic disease: New York, Nova Science Publishers, Inc. p. 128-130.

Luo, X., Bixian, M., Yang, Q., Fu, J., Sheng, G., and Wang, Z., 2004, Polycyclic aromatic hydrocarbons (PAHs) and organocholorine pesticides in water columns from the Pearl River Delta in South China: Marine Pollution Bulletin, v. 48, p. 1102-1115.

MacDonald, D. D., Ingersoll, C. G., and Berger, T. A., 2000, Development and Evaluation of consensus-based sediment quality guidelines for freshwater ecosystems: Archives of Environmental Contamination and Toxicology, v. 39, p. 20-31.

Mahler, B. J., Ingersoll, C. G., Van Metre, P. C. et al., 2015, Acute toxicity of runoff from sealcoated pavement to Ceriodaphnia dubia and Pimephales promelas: Environmental Science and Technology, v. 49, p. 5060-5069.

Mahler, B. J., Van Metre, P. C., Bashara, T. J., et al., 2005, Parking Lot Sealcoat: An unrecognized source of urban polycyclic aromatic hydrocarbons: Environmental Science and Technology, v. 39, p. 5560-5566.

Mahler, B. J., Van Metre, P. C., and Foreman, W. T., 2014, Concentrations of polycyclic aromatic hydrocarbons (PAHs) and azaarenes in runoff from coal-tar- and asphalt-sealcoated pavement: Environmental Pollution, v. 188, p. 81-87.

Martin, L. H. K., Winnefeld, F., Muller, C. J., and Lothenback, B., 2015, Contribution of limestone to the hydration of calcium sulfoaluminate cement: Cement and Concrete Composites, doi: 10.1016/j.cemconcomp.2015.07.005.

Maxted, J. R., and Shaver, E., 1998, The use of retention basins to mitigate stormwater impacts to aquatic life: United States Environmental Protection Agency, National Conference on Retrofit Opportunities for Water Resource Protection in Urban Environments, p. 6-15.

McCarthy, J. F. and Zachara, J. M., 1989, Subsurface transport of contaminants: Environmental Science and Technology, v. 23, p. 496-502.

McKinney, C., 2012, Polycyclic aromatic hydrocarbons and coal-tar sealants: Department of Planning and Development: https://www.ilma-lakes.org/2012/04_PAH_COAL-TAR.pdf.

Missouri Department of Natural Resources, 2015, Geologic hazards in Missouri: Earthquakes, sinkholes, landslides, abandoned mines: http://dnr.mo.gov/pubs/pub2467.pdf.

Missouri State University Campus Facilities, 2016.

Missouri State University Grounds Management, 2016.

Motelay-Massei, A., Ollivan, D., Garban, B., Teil, M. J., Blanchard, M., and Chevreuil, M., 2004, Distribution and spatial trends of PAHs and PCBs in soils in the Seine River sediment basin, France: Chemosphere, v. 155, issue 4, p. 555-565.

National Cooperative Soil Survey, 2004; Wanda Series: https://soilseries.sc.egov.usda.gov/OSD_Docs/W/WANDA.html.

National Cooperative Soil Survey, 2006; Creldon Series: https://soilseries.sc.egov.usda.gov/OSD_Docs/C/CRELDON.html.

National Research Council (US) Committee on Pyrene and Selected Analogues, 1983, Polycyclic Aromatic Hydrocarbons: Evaluation of Sources and Effects. Washington (DC): National Academies Press (US) https://www.ncbi.nlm.nih.gov/books/NBK217760/.

Newell, R. G., and Rogers, K., 2003, The U.S. experience with the phasedown of lead in gasoline: http://web.mit.edu/ckolstad/www/Newell.pdf.

New Jersey Department of Environmental Protection, 2014, Data quality assessment and data usability evaluation technical guidance: http://www.nj.gov/dep/srp/guidance/srra/data_qual_assess_guidance.pdf.

Oakley, S. M., Nelson, P. O., and Williamson, K. J., 1981, Model of trace-metal partitioning in marine sediments: Environmental Science and Technology, v. 15, p. 474-480.

Owen, M. R., Pavlowsky, R. T., and Womble, P. J., 2013, Historical disturbance and contemporary floodplain development along an Ozark River, Southwest Missouri: Physical Geography, v. 32.5, p. 423-444.

Paul, M. J., and Meyer, J. L., 2001, Streams in the urban landscape: Annual Review of Ecology and Systematics, v. 32, p. 333-365.

Pavlowsky, R. T., 2012, Baseline study of PAH sources and concentrations in pond and stream sediments, Springfield, Missouri: Ozarks Environmental and Water Resources Institute.

Pavlowsky, R. T., 2013, Coal-tar pavement sealant use and polycyclic aromatic hydrocarbon contamination in urban stream sediments: Physical Geography, v. 34, p. 392-415.

Philips Innovation Services, 2013.

Pies, C., Yang, Y., and Hofmann, T., 2007, Distribution of polycyclic aromatic hydrocarbons (PAHs) in floodplain soils of the Mosel and Saar River: Journal of Soils and Sediments, v. 7, issue 4, p. 216-222, doi: http://dx.doi.org/10.1065/jss2007.06.233

Piskonen, R. and Itavaara, M., 2004 Evaluation of chemical pretreatment of contaminated soil for improved PAH bioremediation: Environmental Biotechnology, v. 65, p. 627-634.

Quantin C., Joner, E. J., Portal, J. M., and Berthelin, J., 2004, PAH dissipation in a contaminated river sediment under oxic and anoxic conditions: Environmental Pollution, v. 134, p. 315-322.

Readman, J. W., Fillmann, G., Tolosa, I., et al., 2002, Petroleum and PAH contamination of the Black Sea: Marine Pollution Bulletin, v. 44, p. 48-62.

Ritchie, J. C. and McHenry, R. J., 1990, Application of Radioactive fallout Cesium-137 for measuring soil erosion and sediment accumulation rates and patterns: A review: Journal of Environmental Quality, v. 19, issue 2, p. 215-233.

Rogerson, P.A., 2010. Statistical Methods for Geography: A Student's Guide, Third Edition. Sage Publications Ltd.

Santschi, P.H., Presley, B. J., Wade, T. L., Garcia-Romero, B., and Baskaran, M., 2001, Historical contamination of PAHs, PCBs, DDTs, and heavy metals in Mississippi River Delta, Galveston Bay and Tampa Bay sediment cores: Marine Environmental Research, v. 52, p. 51-79.

Silberg, M. S., 2010, Principles of General Chemistry, Second Edition: McGraw-Hill, p. 14-17.

Srogi, K., 2007, Monitoring of environmental exposure to polycyclic aromatic hydrocarbons: a review: Environmental Chemistry Letters, v. 5, p. 169-195.

Star-Seal of Florida Inc., 2014, Guidelines for sealcoating: http://www.starsealfl.com/guidelines/.

Syrovetnik, K., Malmstrom, M.E., and Neretnieks, I., 2007, Accumulation of heavy metals in the Oostriku peat bog, Estonia: Determination of binding processes by means of sequential leaching: Environmental Pollution, v. 147, p. 291-300.

Tessier, A. P., Campbell, P. G. C., and Bisson, M. X., 1979, Sequential extraction procedure for the speciation of trace metals: Analytical Chemistry, v. 51, doi: 10.1021/ac50043a017.

United States Department of Agriculture (USDA), 2016, Soil Surveys for Missouri; Natural Resources Conservative Service Soils: https://www.nrcs.usda.gov/wps/portal/nrcs/surveylist/soils/survey/state/?stateId=MO

USGS, 2011, Coal-tar-based pavement sealcoat, polycyclic aromatic hydrocarbons (PAHs), and environmental health. USGS science for a changing world, doi: https://pubs.usgs.gov/fs/2011/3010/pdf/fs2011-3010.pdf.

USGS, 2015, Coal tar sealant largest source of PAHs in lakes.USGS science for a changing world, doi: https://water.usgs.gov/nawqa/home_maps/sealcoat.html.

USGS, 2016, Determining water-quality trends using sediment cores, White Rock Lake, Dallas: USGS science for a changing world, doi: https://pubs.usgs.gov/circ/circ1171/html/cores.htm.

Van Metre, P. C., and Mahler, B. J., 2013, PAH concentrations in lake sediment decline following ban on coal-tar-based pavement sealants in Austin, Texas: Environmental Science and Technology, v. 48, p. 7444-7228.

Van Metre, P. C., Majewski, M. S., Mahler, B. J., et al., 2012, PAH volatilization following application of coal-tar-based pavement sealant: Atmospheric Environment, v. 51, p. 108-115.

Vittala, S. S., Govindaiah, S., and Gowda, H. H., 2008, Prioritization of sub-watersheds for sustainable development and management of natural resources: An integrated approach using remote sensing, GIS and socio-economic data: Current Science, v. 95, p. 345-354.

Walsh, C. J., Fletcher, T. D., and Ladson, A. R., 2005, Stream restoration in urban catchments through redesigning stormwater systems: looking to the catchment to save the stream: Journal of the North American Benthological Society, v. 24, p. 690-705.

Wang, X. L., Tao, S., Dawson, R. W., and Xu, F. L., 2002, Characterizing and comparing risks of polycyclic aromatic hydrocarbons in the Tainjin wastewater-irrigated area: Environmental Research, v. 90, issue, 3, p. 201-206.

Westerman, D. A., Gillip, J. A., Richards, J. M., et al., 2016, Altitudes and thicknesses of hydrogeologic units of the Ozark Plateaus Aquifer system in Arkansas, Kansas, Missouri, and Oklahoma: U.S. Geological Survey Scientific Investigations Report 2016–5130, 32 p., http://dx.doi.org/10.3133/sir20165130.

Witt, E. C. III, Shi, H., Wronkiewicz, D. J., and Pavlowsky, R. T., 2014, Phase partitioning and bioaccessibility of Pb in suspended dust from unsurfaced roads in Missouri---A potential tool for determining mitigation response: Atmospheric Environment, v.88, p. 90-98.

Wolska, L., Gaier, K., and Namiesnik, J., 2002, Transport and speciation of PAHs and PCBs in a river ecosystem: Polish Journal of Environmental Studies, v. 12, issue 1, p. 105.

Xiao, R., Bai, J., Wang, Q., Gao, H., Huang, L., and Liu, X., 2011. Assessment of heavy metal contamination of wetland soils from a typical aquatic-terrestrial Ecotone in Haihe River Basin, North China. Clean – Soil, Air, Water, v. 39, p. 612-618.

Yang, Y., Ligouis, B., Pies, C., Grathwohl, and Hoffman, T., 2008, Occurrence of coal and coal-derived particle-bound polycyclic aromatic hydrocarbons (PAHs) in a river floodplain soil: Environmental Pollution, v. 151, p. 121-129.

Yang, Y., Van Metre, P. C., Mahler, B. J., et al., 2010, Influence of coal-tar sealcoat and other carbonaceous materials on polycyclic aromatic hydrocarbon loading in urban watershed: Environmental Science and Technology, v. 44, p. 1217-1223.

APPENDICES

Appendix A - PAH Concentrations

Appendix A-1 - 2015 Sediment Samples PAH Concentrations

Date Sampled	Sample	Concentration (ppb)	Location
11/13/2015	1	258,150	SW
11/13/2015	2	537,250	SW
11/13/2015	3	93,400	SW
11/13/2015	4	9,855	SW
11/13/2015	5	15,235	SW
11/13/2015	6	3,280	S
11/13/2015	7	5,240	S
11/13/2015	8	3,520	S
11/13/2015	9	41,100	S
11/13/2015	10	3,360	S
11/13/2015	11	357,500	SE
11/13/2015	12	712,500	SE
11/13/2015	13	7,580	SE
11/13/2015	14	61,750	SE
11/13/2015	15	8,680	SE
11/13/2015	16	5,445	SE
11/13/2015	17	47,750	SE
11/13/2015	18	80,500	SE
11/13/2015	19	94,200	SE
11/13/2015	20	295,900	SE
11/13/2015	21	95,500	SE
11/13/2015	22	44,900	SE
11/13/2015	23	60,800	SE
11/13/2015	24	100,300	SE
11/13/2015	25	17,255	Central
11/13/2015	26	43,300	Central
11/13/2015	27	90,200	Central
11/13/2015	28	200,400	Central
11/13/2015	29	35,200	Central
11/13/2015	30	3,485	Central

Appendix A-2 - 2016 Sediment Sample PAH Concentrations

Date Sampled	Sample	Concentration (ppb)	Core	Core depth (cm)
9/1/2016	31	79,450	1	0-3
9/1/2016	32	54,450	1	3_15
9/1/2016	33	72,700	1	15-20
9/1/2016	34	61,150	1	20-25
9/1/2016	35	12,950	1	25-27
9/1/2016	36	220,600	2	0-5
9/1/2016	37	136,200	2	5_10
9/1/2016	38	48,250	2	10_15
9/1/2016	39	29,290	2	15-20
9/1/2016	40	37,330	2	20-25
9/1/2016	41	21,670	2	25-30
9/1/2016	42	206,300	3	0-10
9/1/2016	43	119,400	3	10_15
9/1/2016	44	51,400	3	15-20
9/1/2016	45	9,250	3	20-25
9/1/2016	46	3,200	3	25-30
9/1/2016	47	3,200	3	30-34
9/1/2016	48	3,200	3	34-35
9/2/2016	49	65,700	N/A	N/A
9/2/2016	50	35,450	N/A	N/A
9/2/2016	51	15,300	N/A	N/A
9/2/2016	52	9,940	N/A	N/A
9/5/2016	53	534,650	N/A	N/A
9/5/2016	54	73,450	N/A	N/A

Appendix A-3- 2015 Individual PAHs with 2-3 Benzene Rings (ppb)

2015 Samples	Ace	Any	Ant	Flu	Nap	Phe
1	1,650	1,650	1,650	1,650	1,650	14,000
2	1,850	1,850	1,850	1,850	1,850	32,000
3	2,100	2,100	2,100	2,100	2,100	2,100
4	205	205	205	205	205	205
5	205	205	205	205	205	205
6	205	205	205	205	205	205
7	210	210	210	210	210	210
8	220	220	220	220	220	220
9	220	220	220	220	220	1,200
10	210	210	210	210	210	210
11	1,800	1,800	1,800	1,800	1,800	25,000
12	1,900	1,900	1,900	1,900	1,900	38,000
13	210	210	210	210	210	210
14	230	230	230	230	230	1,700
15	220	220	220	220	220	220
16	215	215	215	215	215	215
17	250	250	250	250	250	1,300
18	2,500	2,500	2,500	2,500	2,500	2,500
19	2,200	2,200	2,200	2,200	2,200	4,900
20	3,400	3,400	3,400	3,400	3,400	18,000
21	3,350	3,350	3,350	3,350	3,350	3,350
22	2,300	2,300	2,300	2,300	2,300	2,300
23	2,200	2,200	2,200	2,200	2,200	2,200
24	1,850	1,850	1,850	1,850	1,850	8,200
25	195	195	195	195	195	740
26	1,750	1,750	1,750	1,750	1,750	1,750
27	2,600	2,600	2,600	2,600	2,600	2,600
28	2,400	2,400	2,400	2,400	2,400	16,000
29	2,200	2,200	2,200	2,200	2,200	2,200
30	205	205	205	205	205	205

Appendix A-4 2015 Individual PAH concentrations with 4-6 Benzene Rings (ppb)

2015 Samples	BaA	BaP	BbF	BghiP	BkF	Chr	DahA	Fth	InP	Py
1	14,000	21,000	24,000	18,000	24,000	29,000	5,900	41,000	18,000	41,000
2	40,000	48,000	55,000	39,000	43,000	55,000	15,000	85,000	37,000	79,000
3	5,200	7,900	9,000	8,100	8,600	9,500	2,100	12,000	7,400	11,000
4	470	900	1,100	1,000	830	1,000	205	1,100	920	1,100
5	700	1,400	2,000	1,400	1,600	1,700	205	1,900	1,300	1,800
6	205	205	205	205	205	205	205	205	205	205
7	210	210	520	430	420	500	210	640	210	630
8	220	220	220	220	220	220	220	220	220	220
9	1,900	4,200	4,900	3,900	4,300	5,000	1,200	5,000	3,600	4,800
10	210	210	210	210	210	210	210	210	210	210
11	23,000	32,000	34,000	23,000	29,000	37,000	7,500	61,000	22,000	55,000
12	42,000	59,000	72,000	61,000	55,000	74,000	17,000	110,000	55,000	120,000
13	210	650	800	650	610	780	210	900	630	880
14	2,900	5,700	7,900	7,700	5,600	6,500	1,700	7,300	6,600	7,000
15	220	750	1,100	800	750	900	220	950	750	920
16	215	215	570	590	430	460	215	490	490	480
17	2,200	4,800	5,600	5,900	4,600	4,900	1,400	6,000	4,700	5,100
18	2,500	6,300	8,400	7,300	6,000	7,600	2,500	9,500	6,500	8,900
19	5,000	6,900	8,700	7,200	6,800	9,000	2,200	13,000	6,500	13,000
20	16,000	23,000	31,000	21,000	20,000	31,000	6,900	47,000	20,000	45,000
21	3,350	6,700	10,000	7,900	6,800	9,100	3,350	11,000	7,200	10,000
22	2,300	2,300	4,600	2,300	2,300	2,300	2,300	5,200	2,300	5,200
23	2,200	4,600	5,700	5,000	4,400	5,400	2,200	6,600	4,600	6,900
24	5,700	7,000	7,800	6,400	6,800	9,300	1,850	16,000	6,000	16,000
25	980	1,500	1,900	1,300	1,400	1,800	460	2,400	1,300	2,500
26	1,750	1,750	4,400	1,750	1,750	4,600	1,750	6,500	1,750	6,800
27	2,600	6,800	8,600	6,300	6,600	9,200	2,600	13,000	5,900	13,000
28	12,000	15,000	19,000	12,000	12,000	20,000	2,400	34,000	12,000	34,000
29	2,200	2,200	2,200	2,200	2,200	2,200	2,200	2,200	2,200	2,200
30	205	205	205	205	205	205	205	205	205	410

Appendix A-5- 2016 Individual PAHs with 2-3 Benzene Rings (ppb)

2016 Samples	Ace	Any	Ant	Flu	Nap	Phe
31	230	230	230	5,800	7,600	1,600
32	2,250	2,250	2,250	2,250	4,800	2,250
33	2,300	2,300	2,300	2,300	6,500	2,300
34	2,250	2,250	2,250	2,250	4,500	2,250
35	210	210	210	680	1,200	210
36	2,600	2,600	2,600	11,000	20,000	2,600
37	2,250	2,250	2,250	6,900	12,000	2,250
38	2,350	2,350	2,350	2,350	2,350	2,350
39	240	240	240	1,500	2,600	590
40	260	260	260	2,000	3,100	630
41	245	245	245	1,100	1,600	245
42	2,050	2,050	2,050	14,000	12,000	2,050
43	2,000	2,000	2,000	7,700	6,600	2,000
44	2,000	2,000	2,000	2,000	2,000	2,000
45	200	200	200	470	790	200
46	200	200	200	200	200	200
47	200	200	200	200	200	200
48	200	200	200	200	200	200
49	2,200	2,200	2,200	2,200	2,200	2,200
50	1,650	1,650	1,650	1,650	1,650	1,650
51	900	900	900	900	900	900
52	220	220	220	520	660	220
53	1,650	1,650	1,650	20,000	47,000	7,400
54	1,650	1,650	1,650	1,650	4,800	1,650

Appendix A-6- 2016 Individual PAHs with 4-6 Benzene Rings (ppb)

2016 Samples	BaA	BaP	BbF	BghiP	BkF	Chr	DahA	Fth	InP	Py
31	230	3,700	230	11,000	9,000	5,400	7,600	12,000	6,800	7,800
32	2,250	2,250	2,250	7,100	5,900	2,250	4,600	7,300	2,250	2,250
33	2,300	2,300	2,300	9,200	7,800	2,300	6,300	10,000	5,900	6,300
34	2,250	2,250	2,250	8,100	6,700	2,250	5,100	7,400	4,600	4,500
35	210	430	210	1,800	1,500	680	1,200	1,900	1,100	1,200
36	2,600	9,000	2,600	33,000	27,000	12,000	22,000	33,000	19,000	19,000
37	2,250	4,800	2,250	19,000	16,000	8,000	13,000	19,000	12,000	12,000
38	2,350	2,350	2,350	6,300	5,300	2,350	2,350	6,100	2,350	2,350
39	240	1,100	240	4,300	3,700	1,900	2,900	4,200	2,700	2,600
40	260	1,600	260	5,900	4,900	2,600	3,900	5,200	3,400	2,800
41	245	1,200	245	3,600	3,000	1,500	2,100	2,800	1,800	1,500
42	2,050	10,000	2,050	33,000	28,000	14,000	22,000	32,000	19,000	10,000
43	2,000	5,600	2,000	19,000	15,000	7,700	12,000	18,000	11,000	4,800
44	2,000	2000	2,000	7,100	6,000	2000	4,700	7,500	4,100	2,000
45	200	200	200	1,200	990	600	900	1,300	820	780
46	200	200	200	200	200	200	200	200	200	200
47	200	200	200	200	200	200	200	200	200	200
48	200	200	200	200	200	200	200	200	200	200
49	2,200	2,200	2,200	12,000	8,900	2,200	6,800	9,200	4,600	2,200
50	1,650	1,650	1,650	5,500	4,200	1,650	1,650	4,300	1,650	1,650
51	900	900	900	900	1,800	900	900	900	900	900
52	220	460	220	1,500	1,200	600	930	1,300	780	670
53	1,650	24,000	1,650	92,000	78,000	27,000	56,000	76,000	52,000	47,000
54	1,650	5,200	1,650	11,000	11,000	4,800	7,300	7,700	5,400	4,700

Appendix A-7- Detention basin elevation with corresponding PAH concentration

Sample	Basin	Elevation (meters above sea level)	Concentration (ppb)
1	SW	396.225	258,150
2	SW	396.357	537,250
3	SW	396.455	93,400
4	SW	396.495	9,855
5	SW	396.443	15,235
6	S	396.150	3,280
7	S	395.945	5,240
8	S	396.153	3,520
9	S	395.592	41,100
10	S	395.799	3,360
11	SE	395.358	357,500
12	SE	395.366	712,500
13	SE	395.648	7,580
14	SE	395.570	61,750
15	SE	395.676	8,680
16	SE	395.772	5,445
17	SE	395.535	47,750
18	SE	395.399	80,500
19	SE	395.285	94,200
20	SE	395.245	295,900
21	SE	395.248	95,500
22	SE	395.613	44,900
23	SE	395.507	60,800
24	SE	395.319	100,300
25	Central	396.269	17,255
26	Central	395.907	43,300
27	Central	396.776	90,200
28	Central	395.672	200,400
29	Central	396.200	35,200
30	Central	396.364	3,485

Appendix A-8- Coal-tar and Asphalt sealant averages from two previous studies (Mahler et al., 2014; Pavlowsky, 2012)

EPA_{16}	Coal-tar Average (%)	AS Average (%)
Nap	0.32	1.51
Any	0.03	0.06
Ace	0.94	1.50
Flu	1.27	1.85
Phe	14.35	14.86
Ant	3.17	2.58
Fth	21.77	19.45
Py	15.37	13.36
BaA	6.01	6.07
Chr	9.32	8.80
BbF	11.38	10.74
BkF	3.22	3.84
BaP	6.51	6.86
InP	2.44	4.00
DahA	0.61	0.70
BghiP	2.34	3.53

Appendix B – Metal Contamination Analysis

Appendix B-1- 2015 Sediment Sample's Metal Contamination

2015 Samples	Pb (ppm)	Zn (ppm)	Cu (ppm)	Fe (ppm)	Mn (ppm)	Ca (ppm)
1	69	166	< DL	28,776	545	113,898
2	55	122	< DL	22,150	792	39,133
3	78	244	< DL	18,163	434	25,391
4	29	56	< DL	16,274	586	3,435
5	64	94	10	17,463	207	6,706
6	36	53	< DL	23,597	616	2,882
7	57	76	< DL	19,785	623	2,327
8	65	80	< DL	19,572	664	3,501
9	< DL	115	< DL	21,066	433	11,063
10	35	73	< DL	21,581	518	3,841
11	75	413	153	21,257	679	157,213
12	135	447	< DL	17,647	288	221,978
13	53	78	< DL	20,958	727	2,979
14	51	157	11	20,572	454	24,955
15(1)	41	88	< DL	23,322	476	5,835
15(2)	53	92	< DL	24,171	475	5,391
16	52	107	< DL	24,249	642	14,989
17	75	283	25	18,387	223	41,524
18	98	622	86	20,219	403	101,191
19	100	590	122	31,098	361	171,210
20	63	632	86	17,145	94	245,052
21	87	673	169	18,272	236	142,267
22	87	329	28	19,500	347	61,914
23	93	470	52	18,513	428	71,805
24	56	655	73	25,856	443	188,860
25	77	195	18	20,872	446	38,721
26	53	251	21	19,366	355	197,374
27	78	1,019	240	29,900	320	161,371
28	69	439	279	21,844	396	140,559
29	107	211	21	18,892	481	26,425
30(1)	102	174	14	21,516	484	14,032
30(2)	98	159	12	20,655	420	11,077

Appendix B-2- 2016 Sediment Sample's Metal Contamination

2016 Samples	Pb (ppm)	Zn (ppm)	Cu (ppm)	Fe (ppm)	Mn (ppm)	Ca (ppm)
31	71	429	37	20,792	660	60,132
32	111	541	53	30,154	1,087	73,460
33	73	346	31	20,837	798	52,945
34	61	198	20	19,316	894	29,477
35	43	65	< DL	18,889	583	4,547
36	104	541	67	19,367	631	110,488
37	101	432	68	20,747	672	77,229
38	70	180	16	25,198	1,049	34,350
39	62	110	< DL	33,929	715	16,316
40	115	234	17	31,416	336	32,700
41	83	250	33	25,959	136	40,067
42	65	141	< DL	19,487	536	37,085
43	76	145	< DL	20,103	644	41,843
44	62	115	< DL	18,626	518	28,288
45	83	111	< DL	20,020	534	14,415
46(1)	37	51	< DL	16,174	872	4,574
46(2)	39	47	< DL	17,008	1,026	5,414
47	43	47	< DL	20,453	777	5,574
48	< DL	21	< DL	15,646	451	2,592
49	50	597	28	22,698	262	283,687
50	35	570	63	30,126	242	256,284
51	132	643	31	19,871	1,003	10,750
52	95	100	< DL	24,914	480	6,038
53	167	98	< DL	15,019	281	18,484
54	349	574	< DL	28,439	603	136,434

Appendix B-3- 2016 Duplicate Core Metal Contamination

Duplicate Core	Pb (ppm)	Zn (ppm)	Cu (ppm)	Fe (ppm)	Mn (ppm)	Ca (ppm)
31	66	356	43	21,696	909	44,923
32	103	360	33	20,800	845	58,471
33	60	144	13	21,823	854	18,291
34	44	104	10	22,427	866	17,709
35	40	113	15	22,302	630	23,103
36	113	510	72	19,371	531	111,592
37	94	363	52	20,529	576	72,262
38A(1)	76	199	20	23,081	844	37,307
38A(2)	175	218	19	23,659	841	38,718
38B	69	138	< DL	29,188	929	23,673
42	58	143	< DL	18,307	531	32,586
43	62	120	< DL	19,953	551	31,835
44	89	113	< DL	20,444	749	16,898
45	93	129	< DL	24,338	854	13,337
46	111	105	< DL	22,413	957	9,011
47	112	129	< DL	21,514	732	10,152

Appendix B-4- 2015 and 2016 overall determined accuracy

Batch	Pb	Zn	Cu	Fe	Mn	Ca
2016	-1.8	-6.7	-0.2	-4.8	-7.1	-5.1
2015	5.0	-3.9	1.8	-2.1	26.9	-2.3
Average	1.6	-5.3	0.8	-3.4	9.9	-3.7

Appendix B-5- 2015 and 2016 overall determined precision

Batch	Pb	Zn	Cu	Fe	Mn	Ca
2015	14.8	6.7	7.7	3.8	7.2	15.7
2016	42.1	0.5	-2.6	3.8	7.9	10.3
Average	28.4	3.6	2.6	3.8	7.6	13.0

Appendix B-6- 2015 SW sub-basin percentile, minimum, and maximum values

Percentile	Pb	Zn	Cu	Fe	Mn	Ca
min	29	56	10	16,274	207	3,435
10	39	71	10	16,750	298	4,743
25	55	94	10	17,463	434	6,706
50	64	122	10	18,163	545	25,391
75	69	166	10	22,150	586	39,133
90	74	213	10	26,126	710	83,992
max	78	244	10	28,776	792	113,898

Appendix B-7- 2015 Central sub-basin percentiles, minimum and maximum values

Percentile	Pb	Zn	Cu	Fe	Mn	Ca
min	53	174	14	18,892	320	14,032
10	61	185	16	19,129	338	20,229
25	71	199	19	19,743	365	29,499
50	78	231	21	21,194	421	89,640
75	96	392	185	21,762	472	156,168
90	105	729	260	25,872	483	179,373
max	107	1,019	279	29,900	484	197,374

Appendix B-8- 2015 South sub-basin percentiles, minimum and maximum values

Percentile	Pb	Zn	Cu	Fe	Mn	Ca
min	35	53	< DL	19,572	433	2,327
10	35	61	< DL	19,657	467	2,549
25	36	73	< DL	19,785	518	2,882
50	47	76	< DL	21,066	616	3,501
75	59	80	< DL	21,581	623	3,841
90	63	101	< DL	22,791	648	8,174
max	65	115	< DL	23,597	664	11,063

Appendix B-9- 2015 SE sub-basin percentiles, minimum and maximum values

Percentile	Pb	Zn	Cu	Fe	Mn	Ca
min	41	78	11	17,145	94	2,979
10	51	94	24	17,835	227	8,581
25	54	189	34	18,419	303	29,097
50	75	430	80	20,396	416	86,498
75	92	614	113	22,806	471	167,711
90	99	648	155	25,374	668	212,043
max	135	673	169	31,098	727	245,052

Appendix C – Laser Diffraction Particle Size Analysis

Appendix C-1- 2015, 2016, and duplicate core grainsize analysis

Sample ID	Texture (%)					Particle Diameter (μm)		
(code)	% Sand (2,000 - 62.5μm)	%Silt (62.5 - 3.9μm)	%Clay (<3.9μm)	Mean (μm)	Mode (μm)	d10 (μm)	d50 (μm)	d90 (μm)
MSU-1	85.4	10.7	4.0	512.7	517.2	20.1	474.0	1,035.4
MSU-2	58.9	30.7	10.3	403.3	1090.8	3.7	322.4	1,044.8
MSU-3	11.4	67.6	21.0	34.8	23.8	1.6	15.7	73.9
MSU-4	4.1	76.1	19.9	23.2	26.1	1.7	16.3	44.6
MSU-5	9.5	69.6	20.9	31.6	23.8	1.6	15.6	61.0
MSU-6	8.6	69.3	22.1	30.0	26.1	1.5	15.3	56.6
MSU-7	10.5	68.6	20.9	34.0	23.8	1.6	15.8	66.8
MSU-8	8.3	70.7	21.1	30.2	23.8	1.6	15.5	55.0
MSU-9	9.4	69.9	20.8	31.4	26.1	1.6	16.3	60.6
MSU-10(1)	11.0	68.3	20.7	34.9	26.1	1.6	16.3	71.4
MSU-10(2)	5.5	72.4	22.1	23.7	26.1	1.5	14.9	47.7
MSU-11	85.0	10.5	4.5	584.0	824.5	15.0	583.5	1,154.2
MSU-12	83.7	11.8	4.5	478.1	993.6	16.4	415.9	1,015.0
MSU-13	10.8	51.8	37.4	25.9	4.0	0.9	5.9	68.1
MSU-14	10.2	68.1	21.7	31.2	23.8	1.6	15.0	64.8
MSU-15	11.9	66.7	21.5	35.2	26.1	1.6	15.9	77.4
MSU-16	10.8	66.9	22.3	33.6	26.1	1.6	15.4	68.7
MSU-17	7.0	72.0	21.0	26.9	23.8	1.7	15.2	50.8
MSU-18	11.9	70.8	17.4	36.0	28.7	2.0	19.6	71.8
MSU-19	58.0	32.6	9.3	248.6	517.2	4.2	125.2	684.9
MSU-20(1)	62.5	29.0	8.5	208.5	153.8	4.7	116.4	589.9
MSU-20(2)	71.8	21.6	6.6	265.2	203.5	7.5	155.4	713.8
MSU-21	25.3	58.6	16.1	67.9	28.7	2.3	25.5	171.5
MSU-22	22.2	59.6	18.3	71.8	23.8	1.9	18.9	239.7
MSU-23	12.2	70.0	17.8	32.9	26.1	1.9	19.3	75.3
MSU-24	84.2	11.5	4.3	502.6	751.1	16.6	502.4	969.8
MSU-25	17.1	64.6	18.4	54.8	26.1	1.9	20.0	133.9
MSU-26(1)	73.1	20.8	6.1	383.4	751.1	8.5	352.5	856.9
MSU-26(2)	86.6	10.2	3.2	532.2	567.8	28.3	511.9	1,023.2
MSU-27	65.5	26.0	8.6	284.3	517.2	4.8	205.8	730.7
MSU-28	75.1	19.1	5.8	411.6	751.1	10.1	369.6	912.8
MSU-29	6.4	73.7	20.0	24.3	26.1	1.7	16.8	49.3
MSU-30(1)	7.4	70.1	22.5	26.0	23.8	1.5	14.8	51.2

Appendix C-1 Cont.								
MSU-30(2)	8.0	69.7	22.3	26.2	23.8	1.5	14.9	52.8
MSU-31	10.4	70.5	19.1	34.0	26.1	1.7	17.5	65.6
MSU-32	12.6	67.8	19.6	37.9	26.1	1.7	17.6	81.6
MSU-33	10.9	69.7	19.4	35.0	26.1	1.7	17.5	68.2
MSU-34	6.5	72.2	21.3	27.3	26.1	1.5	15.6	50.3
MSU-35	1.3	76.4	22.2	17.8	23.8	1.5	14.4	39.3
MSU-36	21.9	63.1	15.0	46.9	28.7	2.3	24.6	137.0
MSU-37	19.4	62.9	17.8	58.5	26.1	1.9	20.6	166.8
MSU-38	12.5	66.1	21.4	35.3	26.1	1.5	16.4	88.0
MSU-39	11.5	67.0	21.5	33.7	26.1	1.5	16.7	75.5
MSU-40(1)	20.7	61.6	17.8	66.0	26.1	1.9	21.4	184.7
MSU-40(2)	18.6	61.0	20.4	49.2	28.7	1.6	19.5	170.6
MSU-41	24.0	59.2	16.9	82.2	28.7	2.0	23.2	288.3
MSU-42	25.6	56.9	17.5	92.5	23.8	1.9	21.6	359.9
MSU-43	24.8	57.2	18.0	91.9	23.8	1.9	20.9	348.0
MSU-44	20.9	59.7	19.4	84.6	23.8	1.7	18.5	346.2
MSU-45	7.4	68.8	23.8	25.8	23.8	1.4	13.2	49.6
MSU-46	2.6	70.7	26.8	15.9	19.8	1.2	10.6	36.3
MSU-47	2.5	70.2	27.3	15.6	19.8	1.2	10.3	35.6
MSU-48	2.1	68.9	29.0	14.7	19.8	1.1	9.4	34.4
MSU-49	83.8	12.8	3.4	347.9	517.2	25.4	261.9	809.8
MSU-50(1)	71.5	24.2	4.3	247.2	517.2	14.0	155.1	617.5
MSU-50(2)	74.8	21.6	3.7	241.3	223.4	21.0	161.5	584.6
MSU-51	49.3	39.5	11.2	304.8	993.6	3.4	58.7	940.0
MSU-52	12.8	68.3	18.9	36.6	26.1	1.8	17.7	78.2
MSU-53	22.3	60.9	16.8	88.6	26.1	2.1	21.7	311.3
MSU-54	57.7	33.1	9.2	204.2	245.2	4.3	103.6	540.1
MSU-31_split	17.3	64.3	18.4	55.4	26.1	1.8	19.0	135.6
MSU-32_split	13.9	67.1	19.0	36.4	26.1	1.8	18.1	95.4
MSU-33_split	10.1	68.9	21.1	30.1	23.8	1.5	16.3	63.9
MSU-34_split	8.7	69.9	21.4	28.7	23.8	1.5	16.0	56.1
MSU-35_split(1)	6.0	71.8	22.2	23.9	23.8	1.5	15.2	47.7
MSU-35split(2)	8.3	69.8	21.9	32.3	26.1	1.5	15.5	54.8
MSU-36_split	18.2	65.7	16.1	41.4	28.7	2.1	22.3	102.8
MSU-37_split	13.6	67.1	19.3	36.9	26.1	1.7	18.3	85.9
MSU-38A_split	10.0	68.0	22.0	32.2	26.1	1.5	15.8	63.7
MSU-38B_split	11.1	66.4	22.4	37.1	26.1	1.5	15.8	72.1
MSU-42_split	22.5	59.7	17.9	93.6	26.1	1.9	20.7	383.9
MSU-43_split	20.6	60.3	19.1	88.7	23.8	1.8	19.1	344.1
MSU-44_split	6.9	69.3	23.8	29.1	23.8	1.4	13.3	48.9
MSU-45_split	7.9	67.7	24.4	31.7	23.8	1.3	12.9	51.4

Appendix C-1 Cont.								
MSU-46_split	2.5	71.5	25.9	18.3	23.8	1.3	11.6	38.2
MSU-47_split(1)	2.2	72.4	25.4	18.1	23.8	1.3	11.8	37.8
MSU-47split(2)	7.7	68.4	23.9	25.7	23.8	1.4	13.0	50.6

Appendix C-2- Sample duplicate RPD (%)

Sample	%Sand	%Silt	%Clay
10	-66.19	5.87	6.37
20	13.80	-28.90	-25.84
26	16.86	-68.16	-61.91
30	7.87	-0.64	-0.72
40	-10.64	-0.93	13.92
50	4.52	-11.66	-15.87
35_split	32.34	-2.81	-1.42
47_split	110.44	-5.60	-6.30
Average	13.6	-14.1	-11.5

Appendix C-3- Sand Duplicates RPD (%)

ES63	VFS	FS
1	-4.01	4.04
2	0.71	-0.94
3	-4.44	4.62
4	-4.48	4.83
5	-4.05	4.01
Average	-3.254	3.312

ES250	MS
1	2.95
2	3.6
3	3.25
4	3.29
5	4.56
Average	3.53

Appendix D – Organic Mass Loss on Ignition Sample Analysis

Appendix D -1- 2015 Sediment Sample OM-LOI Data

Sample Number	Preburn Total 105 C weight (g)	Preburn sample weight (g)	Preburn weight loss (g)	600 C postburn Total weight	600 C postburn Sample weight	600 C postburn weight loss	WATER weight loss in oven (%)	OM 600 weight loss on ignition (LOI-%)	RPD (%)
MSU1	16.81	5.01	0.04	16.53	4.73	0.28	0.76	5.51	
MSU2	15.86	4.98	0.05	15.58	4.69	0.29	0.96	5.74	
MSU3(1)	17.29	4.95	0.10	16.79	4.44	0.51	2.04	10.23	
MSU3(2)	15.71	4.90	0.1	15.21	4.39	0.51	2.01	10.31	-0.021
MSU4	17.11	4.93	0.09	16.78	4.60	0.33	1.70	6.77	
MSU5	15.40	4.90	0.11	14.88	4.38	0.52	2.12	10.60	
MSU6	16.64	4.91	0.12	16.15	4.41	0.49	2.31	10.09	
MSU7	16.56	4.92	0.09	16.14	4.51	0.42	1.71	8.44	
MSU8	16.57	4.92	0.09	16.11	4.46	0.46	1.86	9.43	
MSU9	17.32	4.89	0.12	16.73	4.30	0.59	2.39	12.04	
MSU10(1)	16.82	4.89	0.12	16.25	4.32	0.57	2.42	11.61	
MSU10(2)	16.18	4.88	0.12	15.62	4.32	0.57	2.36	11.63	-0.16
MSU11	16.42	5.02	0.01	15.96	4.57	0.46	0.25	9.10	
MSU12	16.53	4.96	0.05	16.01	4.45	0.51	0.96	10.37	
MSU13	16.22	4.89	0.11	15.72	4.39	0.50	2.18	10.30	
MSU14	16.90	4.90	0.10	16.34	4.34	0.56	2.09	11.40	
MSU15	16.38	4.90	0.10	15.88	4.40	0.50	2.10	10.30	
MSU16	18.28	4.89	0.11	17.74	4.36	0.54	2.26	10.98	
MSU17	16.18	4.90	0.10	15.61	4.33	0.57	2.10	11.70	

Appendix D-1 cont. 2015 Sediment Sample OM-LOI Data

Sample Number	Preburn Total 105 C weight (g)	Preburn sample weight (g)	Preburn weight loss (g)	600 C postburn Total weight	600 C postburn Sample weight	600 C postburn weight loss	WATER weight loss in oven (%)
MSU18(1)	16.81	4.90	0.11	16.17	4.26	0.64	2.11
MSU18(2)	16.03	4.91	0.11	15.37	4.25	0.66	2.14
MSU19	16.56	4.99	0.06	16.02	4.45	0.54	1.09
MSU20	18.71	4.93	0.08	17.90	4.12	0.81	1.62
MSU21	17.09	4.87	0.14	15.93	3.71	1.16	2.86
MSU22	15.36	4.88	0.13	14.68	4.20	0.68	2.54
MSU23(1)	16.34	4.91	0.10	15.75	4.32	0.59	1.97
MSU23(2)	15.47	4.92	0.11	14.9	4.34	0.57	2.09
MSU24	15.39	5.00	0.03	15.10	4.71	0.29	0.52
MSU25	18.09	4.91	0.10	17.59	4.41	0.49	2.06
MSU26	16.24	5.01	0.02	15.84	4.61	0.40	0.31
MSU27(1)	17.35	4.96	0.07	16.72	4.33	0.63	1.42
MSU27(2)	18.14	4.98	0.07	17.55	4.39	0.59	1.4
MSU28	18.46	4.99	0.05	17.98	4.51	0.48	0.96
MSU29	15.66	4.90	0.10	15.16	4.41	0.50	2.08
MSU30	18.99	4.88	0.12	18.50	4.39	0.49	2.47

Appendix D-2- 2016 Sediment Sample's OM-LOI Data

Sample Number	Preburn Total 105 C weight (g)	Preburn sample weight (g)	Preburn weight loss (g)	600 C postburn Total weight	600 C postburn Sample weight	600 C postburn weight loss	WATER weight loss in oven (%)	OM 600 weight loss on ignition (LOI-%)	RPD (%)
MSU31	17.35	4.96	0.06	16.82	4.42	0.53	1.15	10.74	
MSU32	15.70	4.95	0.06	15.24	4.48	0.47	1.22	9.44	
MSU33	16.30	4.97	0.04	15.88	4.56	0.42	0.76	8.35	
MSU34	16.40	4.96	0.04	16.07	4.64	0.32	0.86	6.53	
MSU35	16.62	4.97	0.03	16.40	4.75	0.22	0.66	4.40	
MSU36	18.12	4.94	0.06	17.48	4.30	0.64	1.28	12.90	
MSU37(1)	16.07	4.95	0.05	15.55	4.43	0.53	0.99	10.63	
MSU37(2)	17.13	4.95	0.05	16.61	4.43	0.52	1.14	10.47	1.52
MSU38	17.37	4.96	0.04	17.02	4.61	0.35	0.87	7.06	
MSU39	15.44	4.94	0.07	15.10	4.61	0.33	1.37	6.73	
MSU40	15.34	4.95	0.06	14.91	4.52	0.42	1.22	8.58	
MSU41	16.47	4.94	0.06	15.98	4.45	0.49	1.29	9.86	
MSU42	18.43	4.96	0.05	18.03	4.56	0.40	0.94	7.98	
MSU43(1)	16.04	4.96	0.04	15.71	4.62	0.34	0.77	6.81	
MSU43(2)	16.20	4.97	0.04	15.86	4.62	0.34	0.76	6.89	-1.29
MSU44	16.45	4.96	0.05	16.16	4.67	0.29	1.01	5.86	
MSU45	19.09	4.97	0.05	18.85	4.73	0.24	0.93	4.82	
MSU46	16.72	4.98	0.04	16.50	4.76	0.22	0.76	4.46	
MSU47	16.72	4.97	0.05	16.52	4.78	0.19	1.04	3.92	
MSU48	16.88	4.97	0.05	16.70	4.79	0.17	0.90	3.52	
MSU49(1)	16.11	5.00	0.01	15.81	4.70	0.31	0.28	6.13	
MSU49(2)	17.32	4.98	0.02	17.02	4.67	0.31	0.49	6.22	-1.54

Appendix D-2- cont. 2016 Sediment Sample's OM-LOI Data

Sample Number	Preburn Total 105 C weight (g)	Preburn sample weight (g)	Preburn weight loss (g)	600 C postburn Total weight	600 C postburn Sample weight	600 C postburn weight loss	WATER weight loss in oven (%)	OM 600 weight loss on ignition (LOI-%)	RPD (%)
MSU50	18.38	4.99	0.01	18.14	4.75	0.24	0.24	4.87	
MSU51	17.01	4.34	0.67	16.48	3.81	0.53	13.32	12.16	
MSU52	15.69	4.90	0.12	14.96	4.17	0.73	2.42	14.89	
MSU53(1)	15.83	4.94	0.07	15.30	4.42	0.52	1.47	10.62	
MSU53(2)	17.7007	4.9552	0.0621	17.1794	4.4339	0.5213	1.2377	10.5203	0.92
MSU54	16.24	4.94	0.06	15.70	4.40	0.54	1.27	10.92	

Appendix D- 3- 2016 Duplicate Core Sediment Samples OM-LOI Data

Sample Number	Preburn Total 105 C weight (g)	Preburn sample weight (g)	Preburn weight loss (g)	600 C postburn Total weight (g)	600 C postburn Sample weight (g)	600 C postburn weight loss (g)	WATER weight loss in oven (%)	OM 600 weight loss on ignition (LOI-%)	RPD (%)
MSU-31	15.75	4.95	0.07	15.23	4.42	0.53	1.33	10.68	
MSU-32	16.86	4.93	0.08	16.38	4.45	0.48	1.62	9.69	
MSU-33	16.59	4.96	0.05	16.28	4.65	0.31	0.96	6.29	
MSU-34	15.43	4.96	0.05	15.15	4.68	0.28	1.07	5.66	
MSU-35	16.61	4.97	0.05	16.37	4.72	0.24	0.99	4.91	
MSU-36	16.21	4.93	0.08	15.54	4.26	0.67	1.58	13.62	
MSU-37(1)	18.72	4.93	0.07	18.16	4.38	0.55	1.42	11.19	
MSU-37(2)	16.51	4.94	0.06	15.94	4.38	0.56	1.25	11.4	-0.47
MSU-38A	17.04	4.94	0.07	16.70	4.60	0.34	1.34	6.79	
MSU-38B	16.52	4.95	0.06	16.21	4.64	0.31	1.27	6.28	
MSU-42	18.13	4.96	0.05	17.73	4.56	0.39	0.94	7.96	
MSU-43	17.18	4.96	0.05	16.85	4.62	0.34	0.92	6.83	
MSU-44	17.39	4.96	0.05	17.13	4.70	0.26	0.90	5.18	
MSU-45(1)	16.53	4.96	0.05	16.28	4.71	0.24	0.93	4.90	
MSU45(2)	16.48	4.95	0.06	16.21	4.68	0.27	1.18	5.49	-2.76
MSU46	16.95	4.96	0.05	16.71	4.72	0.24	0.96	4.79	
MSU47	15.52	4.96	0.05	15.29	4.74	0.22	1.04	4.51	

Appendix E- Basin Elevation Transects

Appendix E-1-2015 SW transect with corresponding sampling locations

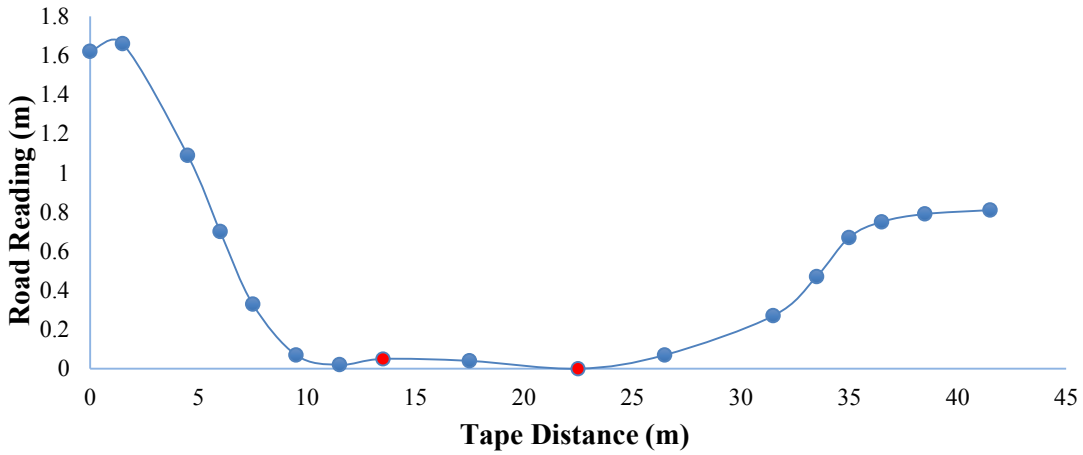

Appendix E-2- South Sub-basin transect with corresponding sampling locations

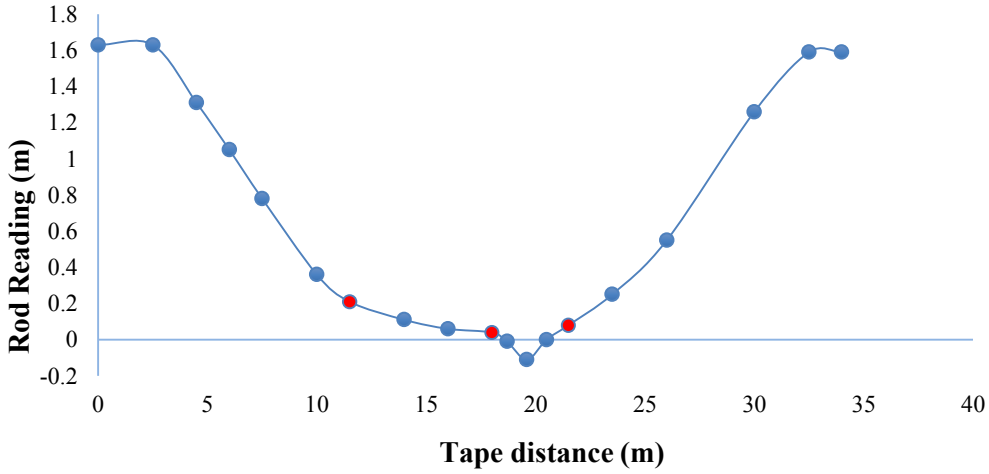

Appendix E-3- South Sub-basin, transect two, with sampling locations

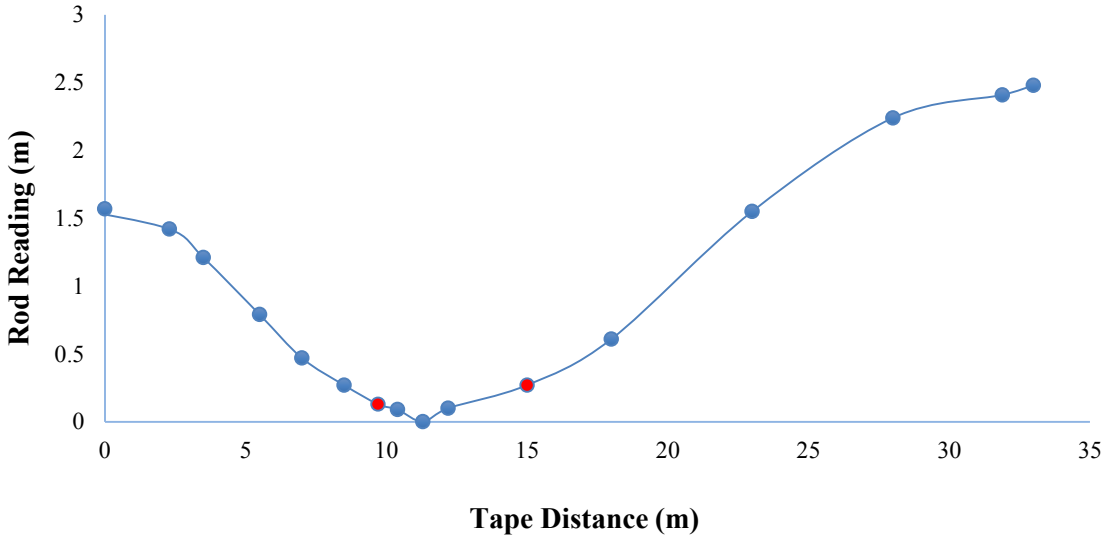

Appendix E-4-SE Sub-basin with corresponding sampling locations

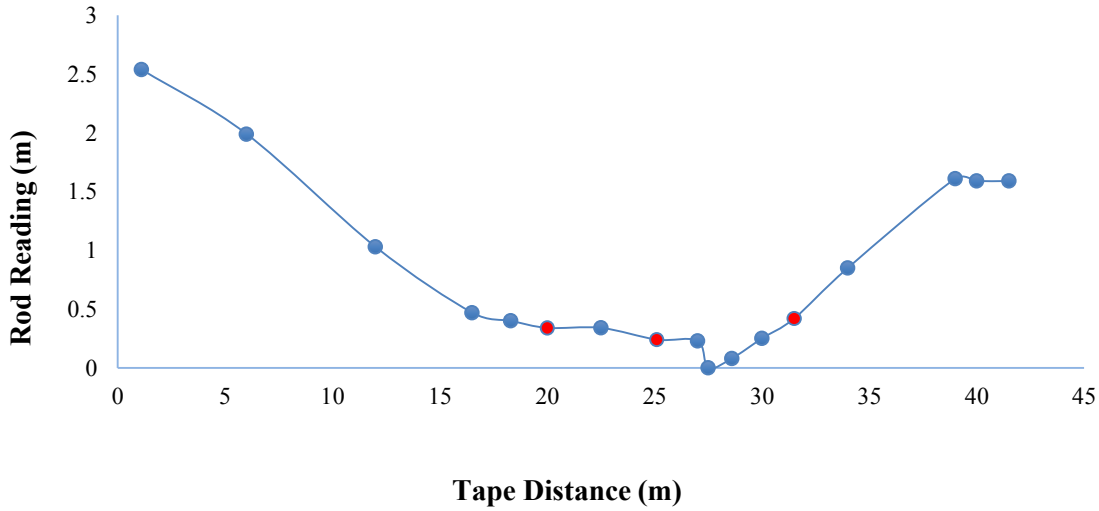

Appendix E-5- SE Sub-basin, transect two, with sampling locations

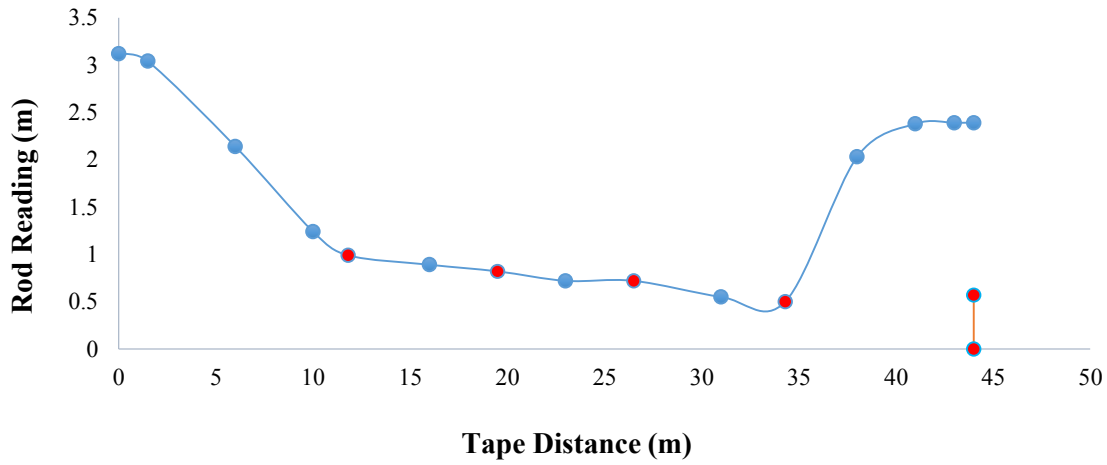

Appendix E-6- SE Sub-basin, transect three, with sampling locations